NONLINEAR MECHANICS OF VISCOELASTIC LAYERED COMPOSITES

A Thesis
Presented to
The Academic Faculty

By

Kashyap Alur

In Partial Fulfillment
Of the Requirements for the Degree
Master of Science in Mechanical Engineering

Georgia Institute of Technology

May, 2015

NONLINEAR MECHANICS OF VISCOELASTIC LAYERED COMPOSITES

Approved by:

Dr. Julien Meaud
School of Mechanical Engineering
Georgia Institute of Technology

Dr. Michael J. Leamy
School of Mechanical Engineering
Georgia Institute of Technology

Dr. H. Jerry Qi
School of Mechanical Engineering
Georgia Institute of Technology

Date Approved: April 16, 2015

Acknowledgements

I would like to thank my advisor Dr. Julien Meaud for introducing me to the research on the nonlinear mechanics of viscoelastic composites. In addition I would like to thank him for his interest, guidance and support throughout the learning process. I would also like to thank my committee members Dr. Michael J. Leamy and Dr. H. Jerry Qi for their time and interest in this thesis.

Contents

List of Tables

List of Figures

Summary

This master's thesis discusses the finite deformation response of viscoelastic parallel plane layered composites. An understanding of their response can aid in the creation of multifunctional materials that optimize stiffness and damping. Such materials could be used in structural applications to dampen vibrations as well as in acoustic applications to absorb sound.

Chapter 1 discusses some fundamental concepts dealing with viscoelasticity. Chapters 2 and 3 provide a literature review on past research that inspired this work as well as the objectives of this research. Chapter 4 provides a detailed overview on the finite element simulations that were done in this research. In Chapter 5 an overview of buckling in elastic composites is provided. This facilitates the understanding of the finite deformation response of viscoelastic composites. Chapter 6 begins the discussion on the finite deformation response by considering constant strain rate loading of both viscoelastic and elastic parallel plane layered composites. Attention is given to the postbuckling response as well as the evolution of buckling due to viscoelasticity. Chapter 7 furthers the discussion to show how the stiffness and damping properties of viscoelastic composites under periodic loading can be tuned. In the final chapter, an outline of possible extensions to this research are provided.

Chapter 1

Introduction

Creating multifunctional materials has been a focus of research for many years [9]. Techniques can been used to create materials that optimize various parameters. Two such parameters that will be the focus of this thesis are stiffness and damping. Generally, a stiff material like steel does not possess very favorable damping characteristics. On the other hand, a viscoelastic polymer does have very high damping, however is not very stiff [2, 20]. To compare materials and get a better understanding of what is attainable, a stiffness loss map, which simultaneously graphs the stiffness and damping of various materials, can be created. An example is shown in Fig. 1.1 [20]. Stiffer materials like steel and other structural metals are shown to the upper left which is characteristic of materials with high stiffness and low damping. Lossy materials like rubber and other polymers are shown to the bottom right which is characteristic of materials with low stiffness and high damping. Ideal materials would possess both high stiffness and high damping and would be situated towards the upper right in this graph. One common way to compare materials is to look at a figure of merit.

A figure of merit is a tool often used in engineering design to convey how 'good' a material is. It can be especially useful when looking at two competing properties, like stiffness and damping. A single number that characterizes both values for a particular material is useful. Chen and Lakes [5] proposed a figure of merit for this case as the product of a materials stiffness and damping. The line for a figure of merit of 0.6 GPa is shown on Fig. 1.1. A material with good simultaneous properties would be situated above this line.

Creating a composite consisting of such materials that optimizes both parameters is of great interest. For example, it could be used in structural applications to dampen vibrations. They would provide the rigidity required while simultaneously attenuating

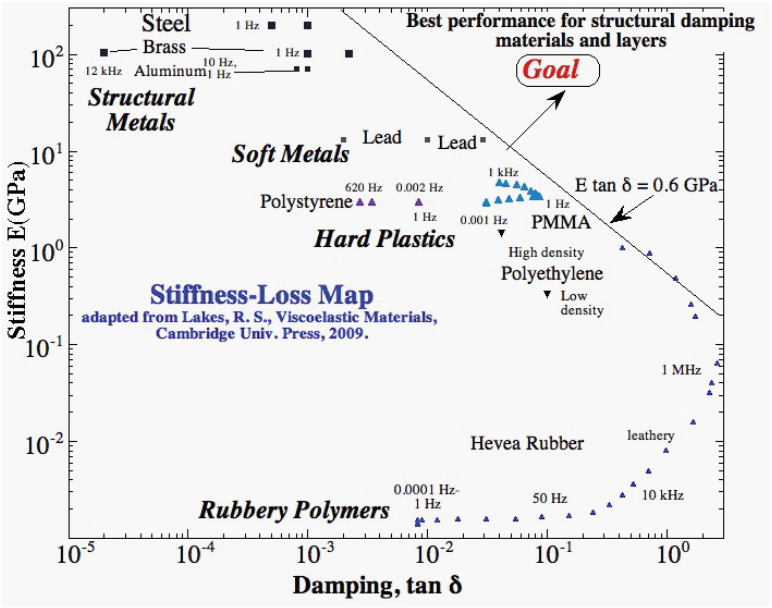

Figure 1.1: Stiffness loss map for various materials [20].

any vibration caused by the surrounding environment (e.g. in a vehicle or machinery). Additionally, such materials could be used to absorb sound as well. Before addressing an in depth literature review on previous research done pertaining to this topic, an overview of pertinent concepts will be covered.

1.1 What is viscoelasticity?

Hooke's law is a common principle that correlates a force with a displacement for linear elastic materials. In the small strain regime Eq. 1.1 shows Hooke's law in terms of stress and strain, which is more applicable in this case, for the one-dimensional case.

$$\sigma = E\epsilon \tag{1.1}$$

σ is the stress, ϵ is the strain and E is the Young's modulus. Elastic materials are often represented as springs as shown in Fig. 1.2A. Viscous materials behave differently in that they are time and rate dependent. The stress-strain relationship for a viscous

material is shown by the following formula:

$$\sigma = \eta \frac{d\epsilon}{dt} \tag{1.2}$$

η, the viscosity, is used to characterize viscous materials. Viscous materials are often represented as dashpots as shown in Fig. 1.2B.

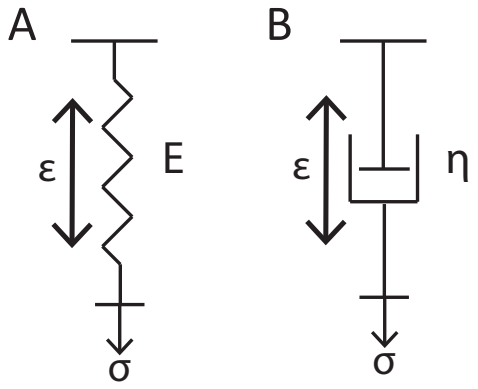

Figure 1.2: A. Elastic spring with stiffness E. B. Dashpot with viscosity η.

A viscoelastic material exhibits characteristics of both elastic and viscous materials and can be described well by two phenomena: creep and stress relaxation. If a viscoelastic material is held under force control it will experience creep. In other words, if a step stress is applied and then held to a viscoelastic material, the strain will continue to gradually increase and eventually converge as shown in Fig. 1.3A. On the other hand, if a step strain is applied and held to a viscoelastic material, it will experience stress relaxation. The stress will gradually decrease and converge as shown in Fig. 1.3B. Both creep and stress relaxation are dependent on the viscosity of the material. Using the latter experiment, the relaxation modulus, $E(t)$, can be obtained.

Viscoelastic materials are generally represented by using springs and dashpots. One common way is to represent them as a standard linear solid, which combines springs and a dashpot in both series and parallel (Fig. 1.4).

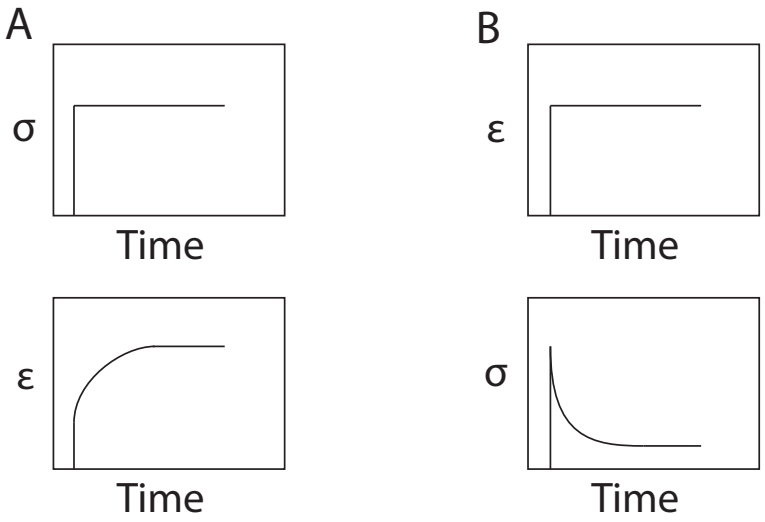

Figure 1.3: A. Creep as a result of a step stress. B. Stress relaxation as a function of step strain.

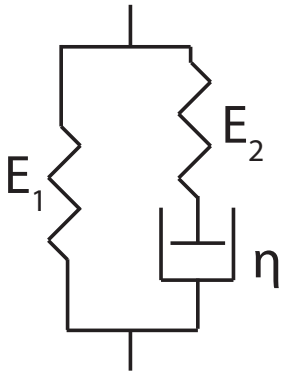

Figure 1.4: Standard linear solid represented using springs and dashpots

Another defining feature of a viscoelastic material is that unlike an elastic material, it dissipates mechanical energy. Under periodic loading, the stress vs. strain response for an elastic material follows the same path while loading and unloading as seen in Fig. 1.5A. The stress vs strain response for a viscoelastic material under dynamic loading is more complex. It is time dependent and does not follow the same path during loading and unloading as seen in Fig. 1.5B. This is because during loading the strain lags the stress (shown in Fig. 1.6). As a result we see damping, or energy dissipation.

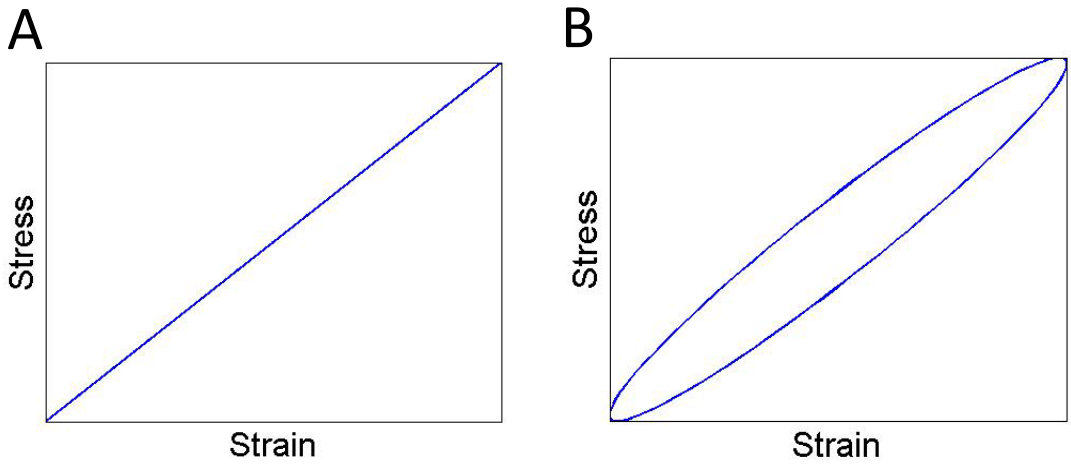

Figure 1.5: A. Elastic stress strain relationship. B. Viscoelastic stress strain relationship.

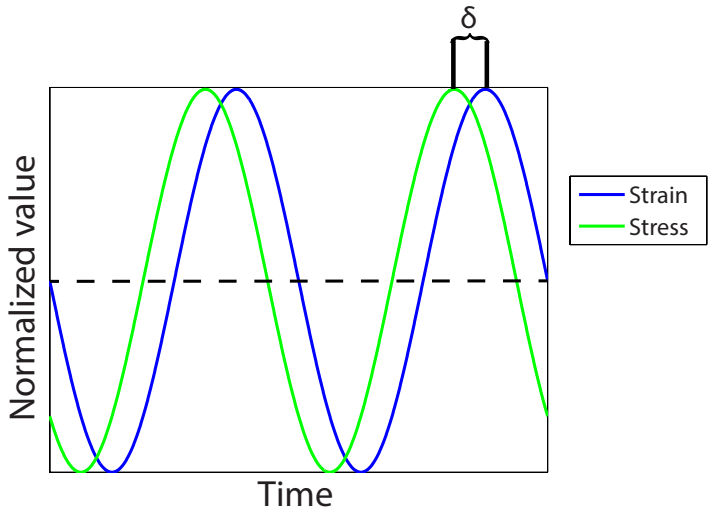

Figure 1.6: Normalized stress and strain response for a linear viscoelastic material, where stress lags the strain

1.2 Stiffness and Damping of Viscoelastic Materials

1.2.1 Stiffness

The stiffness, or Young's modulus, for a linear elastic material is the slope of the stress-strain response (Fig. 1.5A). In the case of a viscoelastic material the stiffness can be defined in multiple ways. For example, consider a situation when it is subject

to a sinusoidal displacement shown by the following equation:

$$\epsilon(t) = \Delta\epsilon \sin(\omega t) = \mathrm{Im}(\Delta\epsilon\, e^{i\omega t}) \tag{1.3}$$

where $\Delta\epsilon$ is the amplitude of loading, and ω is the frequency in radians. The stress response is also sinusoidal as shown in the following equation:

$$\sigma(t) = \Delta\sigma \sin(\omega t + \delta) = \mathrm{Im}(\Delta\epsilon\, e^{i(\omega t+\delta)}) \tag{1.4}$$

where $\Delta\sigma$ is the amplitude of the response, δ is the phase lag between the stress and strain, and ω is the frequency in radians. Because the strain lags the stress the dynamic Young's modulus, E^*, can be written in terms of real and imaginary components shown below:

$$\epsilon^* = \Delta\epsilon\, e^{i\omega t} \tag{1.5}$$

$$\sigma^* = \Delta\sigma\, e^{i(\omega t+\delta)} \tag{1.6}$$

$$E^* = \frac{\sigma^*}{\epsilon^*} \tag{1.7}$$

$$E^* = E' + iE'' \tag{1.8}$$

where E' is the storage modulus and E'' is the loss modulus. One way to define the stiffness is the absolute value of the dynamic Young's modulus, E^*, also written as $|E^*|$. The stiffness of a viscoelastic material may also be defined by its storage modulus, E'. Fig. 1.7 depicts both $|E^*|$ and E' graphically. $|E^*|$ and E' are typically dependent on ω.

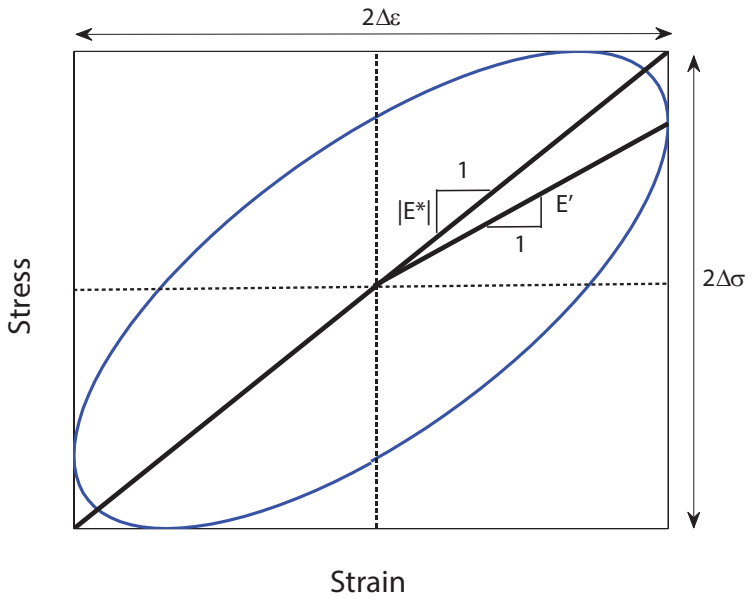

Figure 1.7: Measures of stiffness, $|E^*|$ and E', depicted for a linear viscoelastic material.

1.2.2 Damping

There are several ways to measure damping for a viscoelastic material. One common way to describe the damping of a linear viscoelastic material is by the tangent of the phase lag, or $\tan(\delta)$. The phase lag, δ, can be found graphically as shown in Fig. 1.6. $\tan(\delta)$ can also be found from the loss and storage moduli:

$$\tan(\delta) = \frac{E''}{E'} \tag{1.9}$$

Another common way to describe the damping of a linear viscoelastic material is by considering the energy stored, W_s, and energy dissipated, W_d, per unit volume. To be specific:

$$\tan(\delta) = \frac{2}{\pi}\frac{W_d}{W_s} \tag{1.10}$$

where W_s and W_d are defined as:

$$W_s = \frac{1}{2}E'\epsilon_0^2 \tag{1.11}$$

$$W_d = \frac{\pi}{4}E''\epsilon_0^2 \tag{1.12}$$

It is helpful to note that the energy dissipated per cycle corresponds to the area within the stress-strain response. This definition is useful because it can be used in the case where the stress-strain loop is not an ellipse. This is often seen in the case of nonlinear response, which is covered in more detail in Appendix B.

1.3 Nonlinear Viscoelasticity

Nonlinear behavior can result from either material or geometric nonlinearities. Material nonlinearities refer to a nonlinear stress-strain relationship intrinsic to the material. It is important to realize that while material nonlinearities do become more obvious at high strains, only a very small strain is needed to see the effects. Geometric nonlinearities arise in situations of high displacement or strain. They refer to nonlinearities in the kinematics, like strain-displacement relations. An example of a linear viscoelastic stress-strain response is shown in Fig. 1.8A while a nonlinear response is shown in Fig. 1.8B. The nonlinearities present in the results of this research are due to geometric nonlinearities, and will be dicussed in further detail.

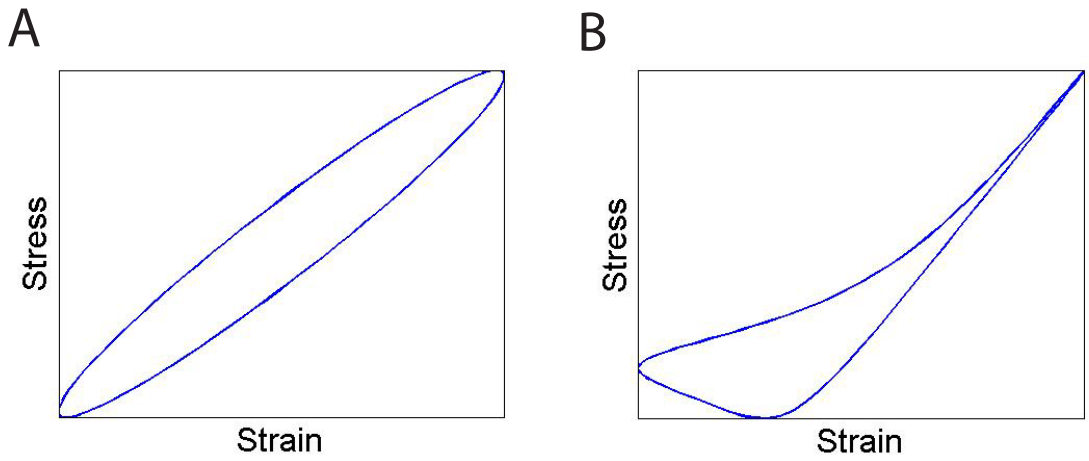

Figure 1.8: A. Linear viscoelastic response. B. Nonlinear viscoelastic response. Differs greatly in tension and compression

Chapter 2

Literature Review

Layered composites are a topic of research in a wide range of fields, and examples are commonly found naturally throughout nature. For example, the imbricated (layered) nature of fish scales are a point of research as they serve several purposes from protection and regeneration to camouflage. Browning et al. [4] experimentally showed that the mechanical response of these layers can be tuned by altering variables such as aspect ratio of the scales, overlap length and angle of the scales. Rudykh and Boyce [31] developed an analytical solution for the same material structure but also focused on the presence of instabilities at high angles. Angles were considered with respect to the horizontal axis while loaded vertically. At lower angles, there is more shearing in the response which decreases the compression in the plates. At higher angles there is less shearing, so buckling is evident at a critical strain . Rudykh and Boyce [32] further developed this idea to utilize localized loading to transform it to large rotational motion. Experiments showed that this can be tuned for given angles and material properties. This literature review will first describe how composite materials with both high stiffness and high damping are attainable, then cover extremal composites and finally provide a review on buckling in layered structures and composites.

2.1 Composites with high stiffness and high damping

Previous research done on the effective stiffness and loss of viscoelastic composites has shown that various variables can be tuned to achieve different characteristics. One such variable is geometry. For layered composites, the geometry is characterized by the angle, θ, between the layer and loading directions. Two simple examples, studied by Chen and Lakes [5], are the Reuss ($\theta = 90$ degree) and Voigt ($\theta = 0$ degree)

geometries, which represent limiting cases. Examples are shown in Fig. 2.1.

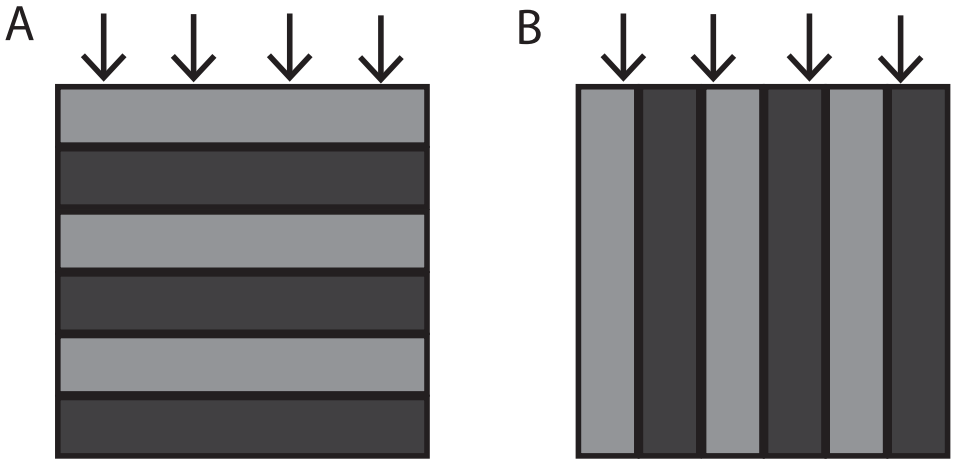

Figure 2.1: A. Two phase Reuss composite. B. Two phase Voigt composite.

Chen and Lakes [5] derived formulae and showed that the Reuss geometry better optimizes stiffness and damping. For small increases in volume fraction of the soft material, there is a significant increase in damping with an insignificant decrease in stiffness. They also proposed that taking advantage of non-affine deformation is one way to create high-loss composites. This will happen as long as the lossy material experiences higher strain than the actual composite does.

Liu et al. [24] investigated the upper and lower bounds on the effective stiffness of a material when the Poisson's ratio was taken into account. They derived formulae to show that for a two phase elastic composite taking into account Poisson effects greatly influences the effective stiffness. Meaud and Hulbert [26] expanded this concept to viscoelastic materials. They found the effective dynamic modulus and loss factors for the Reuss and Voigt topologies when Poisson effects are taken into account by applying the viscoelastic correspondence principle to the equations derived by Liu et al. They also derived equations to relate the tensile and bulk loss factors for a linear viscoelastic material. Their results showed that Poisson effects do not have much of an effect on the stiffness and damping of the Voigt composite. However, the Poisson's ratio and bulk loss factor of the lossy material greatly influence the stiffness

and damping of the Reuss composite.

Layered composites can also be manufactured such that the layers are angled (shown in Fig. 2.2). Meaud et al. [27] derived the effective dynamic properties of layered composites when loaded in an arbitrary direction. This showed that the effective stiffness and damping of the composite depends on the volume fraction of the stiff material and the angle at which the load is applied with respect to the layer direction. Both factors also greatly influence the strains that are experienced by the lossy polymer. They found that simultaneous high damping and high stiffness are achieved when the equivalent strain in the lossy material is large. Additionally, they showed that the 10 degree composite actually displayed better damping and stiffness properties than even the Reuss composite.

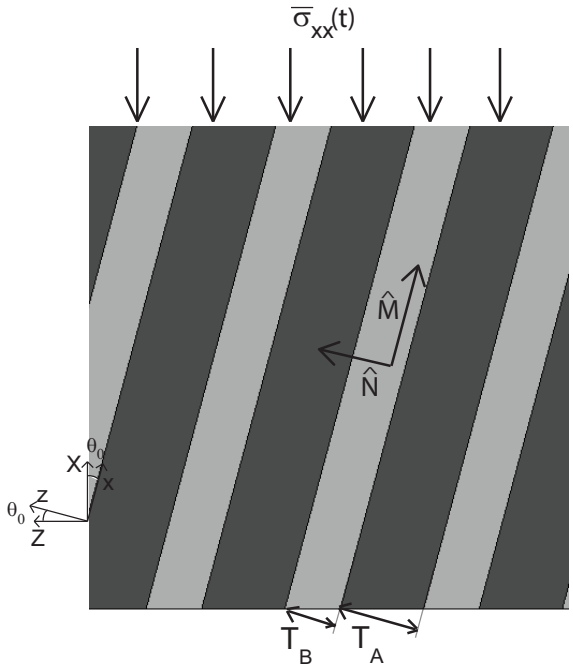

Figure 2.2: Layered composite with materials A and B. T_A and T_B denote the layer thicknesses. The volume fraction of material A is $\phi_A = T_A/(T_A+T_B)$. The x axis and the unit vector $\hat{M}$ are in the layer direction while the z axis and the unit vector $\hat{N}$ are perpendicular to the layer direction. The composite is loaded in the X direction. θ_0 is the angle between the X axis and the layer direction in the undeformed configuration [27].

2.2 Extremal composites

An extremal composite is one which has properties which exceed those of either one of its constituent materials. Research has shown that both extreme stiffness as well as extreme damping are possible as long as the geometries or properties of the constituent materials are chosen or are tuned accordingly.

2.2.1 Negative stiffness for extreme stiffness

When a displacement is applied to a system, there is a resulting reaction force that increases in the opposing direction. Negative stiffness is characterized by a decreasing reaction force, which in essence allows the system to deform even more. Generally a negative stiffness element represents elastic instability. However, it can be made stable if its boundaries are constrained (*i.e.* in a boundary value problem, only displacement boundary conditions are employed) [21]. Studies have shown that composite materials including a negative stiffness element can have a stiffness greater than either one of the constituent materials.

Lakes and Drugan [21] showed theoretically that elastic composites can be much stiffer if a negative stiffness element is included. This is because the local strain in the composite around the negative stiffness element is much larger than the macroscopic applied strain. This results in a large amount of stored energy due to small deformation, which is characteristic of high stiffness.

Jaglinski et. al [16] were able to experimentally test composites made of Barium Titanate in a Tin matrix. They chose their materials such that the inclusions could have a negative bulk modulus when exposed to a certain temperature. The composites underwent cyclic loading resulting in a material with stiffness higher than that of diamond at this temperature.

2.2.2 Extreme damping

Plenty of previous research has been done to design materials that exhibit extreme damping. Both theoretical and experimental results show that extreme damping is indeed possible when negative stiffness elements are introduced into a system. Lakes et al. [22] showed experimentally that extreme damping is possible in composite materials when one of the materials exhibited a negative bulk modulus. They also described a method for creating such a material. Wang and Lakes [34] showed theoretically how a material with a negative bulk modulus is possible and how it can lead to extreme mechanical damping. Wang and Lakes [35] also demonstrated through the use of a discrete lumped parameter model that stable extreme damping is indeed viable by introducing negative stiffness as a geometric nonlinearity.

A bistable buckled beam, like the one shown in Fig. 2.3, is one example of a system that exhibits a geometric nonlinearity. Dong and Lakes [7] created a damper system using PMMA (polymethyl methacrylate) rod, a structural polymer with intrinsic damping properties that can also support large strains. PMMA rods of different lengths (aspect ratio was varied) were placed under sinusoidal loading, and the resultant force and displacement data was gathered. They observed that when the displacement was high, this caused negative stiffness in the response, consequently increasing the damping capacity. Kalathur and Lakes [17] performed similar experiments in which they showed that similar results can be obtained in the small amplitude regime. Additionally, they displayed the time dependent relaxation properties of PMMA. Being viscoelastic, PMMA experiences stress relaxation, so once strained the stiffness decreases as a function of time (Fig. 1.3B). Kashdan et al. [18] also fabricated and experimentally tested a bistable system. They found that in addition to providing an increase in damping, the bistable system allowed for tuning of the dynamic behavior.

Kochmann [19] further enhanced this concept by deriving formulae that model the

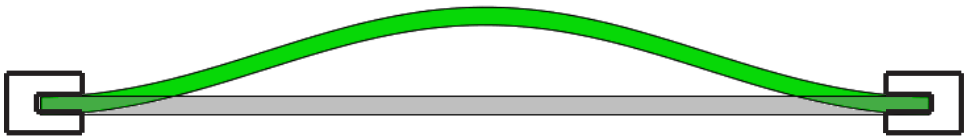

Figure 2.3: Buckled bistable beam. Original configuration shown in gray.

linear viscoelastic response of various linear viscoelastic composite systems near the loss of stability, varying from a one-dimensional spring-dashpot system to a two-phase particle-matrix composite. The formulae considered both the subresonant and resonant regimes and showed that extreme damping is indeed achievable in the presence of nearly unstable constituents.

Fulcher et al. [8] investigated the concept of using bistable buckled beams for shock isolation systems. They conducted experiments observing the various stable buckling modes of the beams. The study of buckling has also been expanded to layered structures and composites as well.

2.3 Buckling in layered structures and composites

Buckling is considered to be an elastic instability, and is commonly considered as a mode of failure for load bearing materials. There has been extensive research done on the viscoelastic response and buckling of fiber-reinforced materials dating all the way back to the 1960's [10, 11, 30]. Rosen's work [30] showed that there are two buckling modes that can occur: the shear and transverse buckling modes shown in Fig. 2.4 [28]. Parnes and Chiskis [28] looked at this concept by studying stiff elastic fiber reinforced composites and drew two conclusions. First, the shear buckling mode will always dominate as a greater stress is needed to observe the transverse buckling mode. Second, for the case of a non-dilute fiber reinforced composites (*i.e.* when the volume fraction of the stiffer constituent is high) the buckling wavelength is infinite, however for a dilute composite (*i.e.* when the volume fraction of the stiffer constituent is small) the buckling wavelength can indeed be a finite value, contrary to what was

proposed by Rosen. Additionally, they also derived formulae to calculate the critical buckling strain, ϵ_{cr}, as well as the critical buckling wavelength, L_{cr}.

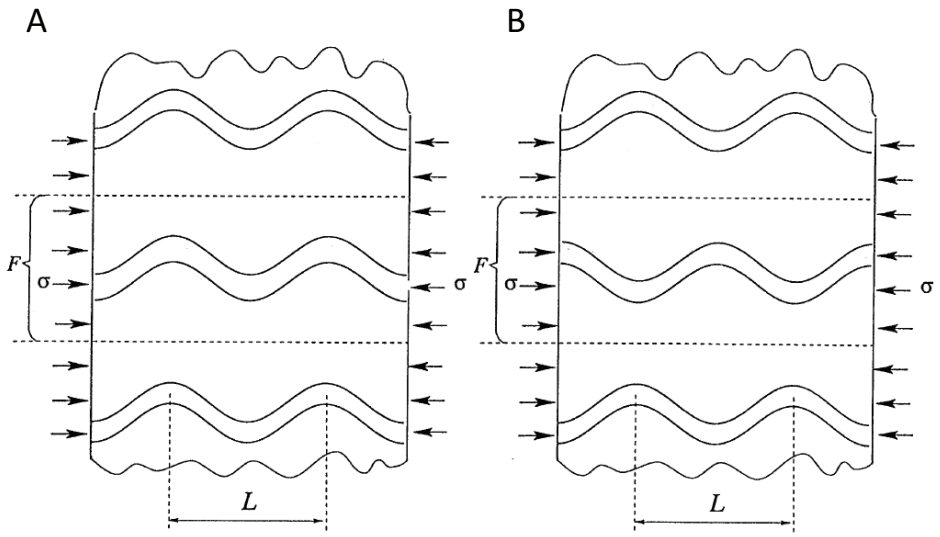

Figure 2.4: A. Shear buckling mode. B. Transverse buckling mode [28].

Recent work has been focused on exploiting buckling to add functionality. Lopez-Pamies and Casteneda [25] studied hyperelastic laminates with the idea that the results can be expanded to more general microstructures. They characterized the response under finite shear deformation and showed that the layer direction can change (as a result of rotation) depending on the initial orientation angle of the composite, potentially leading to a softening mechanism. Rudykh and Boyce [32] investigated using localized loading to induce rotation on hyperelastic materials. They compared experimental and numerical results to show that the initial orientation angle has a great effect on the induced rotation. Li et. al [23] studied the wrinkling of layers in stratified composites. They found that for thin elastic layers, the wrinkling mechanism could be tuned based on various parameters, such as material properties and geometry. Changing either the material stiffness ratio or material thickness ratio (*i.e.* changing from dilute to non-dilute cases) can alter whether the resultant is a long-wave mode (infinite/large wavelength), or wrinkling (small wavelength).

Until now this discussion has been limited to elastic composites. However, there

has been some relevant research done taking into account viscoelasticity in layered structures. Huang and Suo [13, 14] studied the instability and wrinkling of a compressed elastic film on a viscous layer. They derived formulae using nonlinear thin plate theory for the elastic material and the theory of lubrication for the viscous material, to relate the stresses and strains. They formulated an equation to calculate the critical wavenumber for a given strain, as well as the respective growth rate for a given wavenumber. They found that if the initial configuration was perturbed by a wavenumber that was less than the critical wavenumber, the growth rate is positive. If the wavenumber was greater than the critical wavenumber, the wrinkle decays. Growth rate is dependent on the wavenumber because the wavenumber governs the amount of elastic energy that is stored due to bending and the resulting kinetic constraint produced by the viscous layer varies accordingly. The viscous layer controls the amount of time the film may spend in any number of unstable modes before reaching equilibrium [13].

Huang [12] also studied the effect of an elastic thin film on a viscoelastic substrate. Equations were derived to discern the displacements of both layers. With the addition of viscoelasticity the wavelength changed with time, similar to the case of a viscous substrate. The growth rate for a given wavelength was calculated, providing insight into what would be the fastest growing wavelength. Results showed that when perturbed with an initial wavenumber and when the stresses in the layers were not very high, the wrinkle growth was similar to the case of a viscous substrate: the wrinkle grows exponentially, with the fastest growing mode dominating, until the amplitude of the wrinkle eventually reaches an equilibrium value. When the compressive stress is high, the film wrinkles immediately and grows over time. Im and Huang [15] expanded this research to consider a more realistic situation. An initial random perturbation was considered as this is more representative of what might be seen in an experiment. Similar results were examined: the fastest growing mode initially

dominated until an equilibrium state was reached.

Chapter 3

Objectives

As seen in the literature there is a wide range in the buckling response of layered structures. Research has been done to study the response of elastic laminates as well as layered structures with viscoelasticity. However, the objective of this work is to study the finite deformation response of viscoelastic layered composites with parallel plane layers, using the plane strain assumption. To be specific the objective has three parts.

1. Buckling of elastic layered composites. Understanding the buckling modes and critical strains for elastic layered composites aids to get a better understanding on the dynamic response of viscoelastic layered composites. Numerical simulations will be compared with the theoretical formulae that was discussed and derived in Alur and Meaud [1].

2. Finite deformation analysis of viscoelastic layered composites under constant strain rate. This discussion will consider the stress-strain responses and the evolution of buckling due to viscoelastic softening.

3. Finite deformation analysis of viscoelastic layered composites under periodic loading. Using finite element simulations and the formulae derived in [1], there will be a discussion on the nonlinear mechanics of non-dilute composites to show that the stiffness and damping can be tuned.

Chapter 4

Finite Element Modeling

In this thesis viscoelastic layered composite materials consisting of two parallel plane layered constituents are considered. The two layers will be referred to as materials A and B, and Φ_A and Φ_B will correspond to their respective volume fractions. θ is the initial angle with respect to the vertical axis (Fig. 4.1).

This section will include a discussion on the finite element model that was used and a detailed description on all the parameters chosen. Next, the material model and parameters that were chosen will be introduced. Finally, post-processing and analysis techniques will be discussed.

4.1 Finite element model

To conduct the research ABAQUS/CAE Standard, version 6.13 was employed in conjunction with Python scripts to automate the process. Using Python scripts, all model and material parameters could be adjusted with ease. When creating a finite element model there are a few common basic steps: creating the geometry, meshing, applying constraints and applying boundary and loading conditions. Two types of analyses were conducted: buckling and finite deformation. For both analyses, two types of models are considered: models of infinite size, and models of finite height. Before providing details on the analyses a brief overview on the constraints and conditions unique to these infinite size and finite height models will be given.

4.1.1 Models of infinite size

When considering a model of infinite size in finite element analysis, a unit cell can be modeled with height, H, and width, W, pictured in Fig 4.1. Material A is the stiff, elastic constituent, and material B is the soft, viscoelastic constituent. θ is the angle

with respect to the vertical axis.

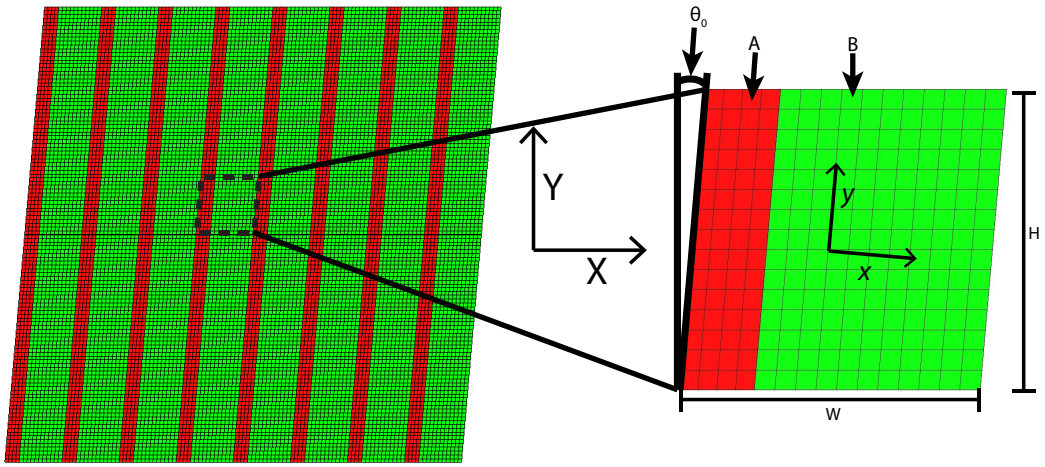

Figure 4.1: Finite element example of a layered composite, zoomed in to show a unit cell.

Periodic boundary conditions were used to model a composite of infinite size. To do this, a Python script was used to create node sets and the appropriate constraints. Node sets were created to group together all the nodes on the outer edges of the model (bottom, top, left and right excluding the corners), as well as separate sets for all of the corners (Fig. 4.2A). Once the groups were created, the script was used to renumber the nodes to facilitate the application of the appropriate constraints, or periodic boundary conditions. They are shown in the equations below.

$$U_Y|_{top} - U_Y|_{bottom} = U_{applied}(t) \tag{4.1}$$

$$U_X|_{top} - U_X|_{bottom} - U_X|_{TL} = 0 \tag{4.2}$$

$$U_Y|_{left} - U_Y|_{right} = 0 \tag{4.3}$$

$$U_X|_{left} - U_X|_{right} - U_X|_{BR} = 0 \tag{4.4}$$

$$U_Y|_{BR} - U_Y|_{BL} = 0 \tag{4.5}$$

$$U_X|_{TR} - U_X|_{BR} - U_X|_{TL} = 0 \tag{4.6}$$

$$U_Y|_{TR} - U_Y|_{BL} = 0 \tag{4.7}$$

U_i is the displacement of the nodes in the i direction, the second set of subscripts refer to the edge or corner (*i.e.* BR = bottom right, BL = bottom left) that the node in question lies on. After application of all the constraints, the appropriate boundary conditions were set. A vertical displacement, $U_{applied}(t)$, was applied to the top left node, the bottom right node was fixed vertically and the displacement of the bottom left node was 0 for all degrees of freedom to prevent rigid body motion as shown in Fig. 4.2A. A possible mode of deformation for these constraints and boundary conditions is shown in Fig. 4.2B.

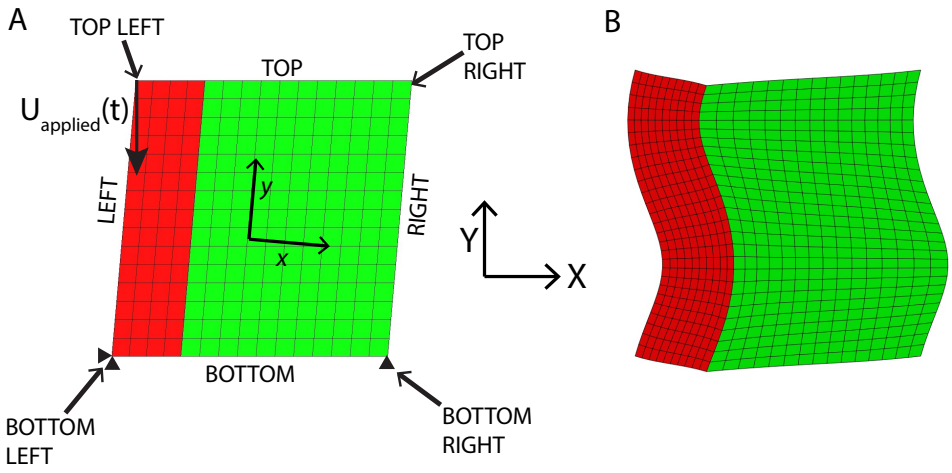

Figure 4.2: A. Boundary conditions shown for a unit cell. B. Corresponding mode of deformation for the unit cell.

4.1.2 Models of finite height

Studying models of infinite size is useful to understand the underlying concepts. However, any manufactured composite would have a finite height. When considering the case for a model with a finite height, the number of layers is assumed to be infinite. A finite width model does not need to be considered because the response of the composite is dependent on the volume fraction of each material and not necessarily on how thick each phase is. For this case, a unit cell was modeled with an appropriate height to width ratio. Periodic boundary conditions were applied only to the left and right edges. In other words only equations 4.3 and 4.4 from before were used. The boundary conditions for this case are also different and are shown below:

$$U_X|_{top} = U_X|_{bottom} = 0 \tag{4.8}$$

$$U_Y|_{top} = U(t) \tag{4.9}$$

$$U_Y|_{bottom} = 0 \tag{4.10}$$

The entire bottom edge is fixed in the vertical and horizontal directions and the

top edge is fixed in the horizontal direction and displaced vertically as shown in Fig. 4.3A. The buckled shape is shown in Fig. 4.3B.

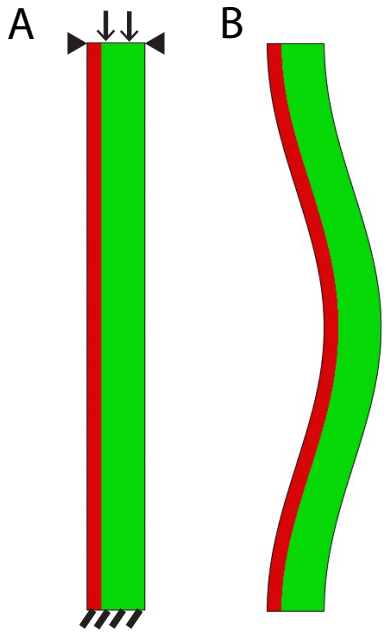

Figure 4.3: A. Example of a finite element model unit cell in ABAQUS with a finite height, shown with boundary conditions. B. Mode of deformation for a model of finite height.

4.1.3 Buckling analysis

To run buckling simulations, the BUCKLE procedure was used in ABAQUS/Standard [6]. The choice of model height is driven by the volume fraction of material A, ϕ_A, since we know that dilute and non-dilute composites buckle with different wavelengths. If the composite buckles with a finite wavelength, L_{cr}[1], the buckling shape is a periodic shape of period L_{cr} in the Y direction. However, a unit cell of height H with periodic boundary conditions can only deform with a periodic shape of period H/i, where i is any positive integer (Fig. 4.4). Therefore, in order to compute the true value for the critical strain, ϵ_{cr}, and L_{cr} using finite element anlaysis, the theoretical values for the buckling wavelength, $L_{cr}|_{th}$, were first calculated using theory derived

[1]The symbol 'L' is used here for the wavelength because λ is used to denote the stretch

in [1]. Buckling simulations were modeled with a unit cell of height $H >> L_{cr}|_{th}$ (typically $H \geq 20 \times L_{cr}|_{th}$). This allows the buckling wavelength predicted by ABAQUS, $L_{cr}|_{FEM}$, to be a discrete value very similar to that of $L_{cr}|_{th}$.

In the case of an infinite buckling wavelength, the height H of the unit cell has no influence on the results, so a height to width ratio, $\frac{H}{W}$, of one was chosen. For all simulations, the width of the unit cell included only one layer of phase A and one layer of phase B since the theory predicts that the shearing mode has a lower critical strain than the transverse mode [28].

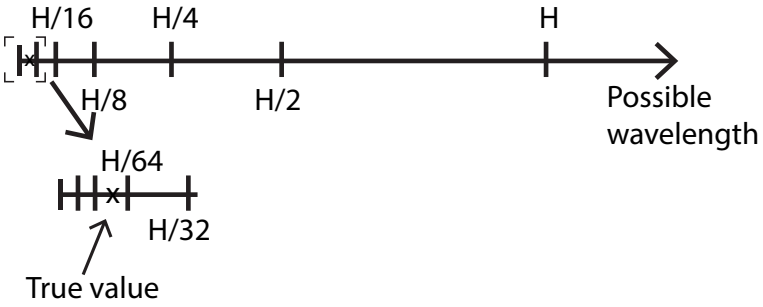

Figure 4.4: Schematic of possible buckling wavelengths for a model with periodic boundary conditions. A taller model ensures that it can more closely capture the true wavelength.

4.1.4 Finite deformation analysis

To run finite deformation analyses, a Dynamic, Implicit step type with nonlinear geometry was used. The same height as the buckling simulations for a given geometry (given volume fraction ϕ_A) was chosen. Imperfections were introduced in order to simulate more realistic situations and can be introduced in several ways. The first method uses results from the buckling simulations by applying the imperfection as a scaled sum of different buckling modes. For most simulations only the first mode is considered because it corresponds to the lowest buckling strain. Imperfections may also be introduced directly to the model by providing coordinate perturbations at both vertical edges of the model as well as at the interface between the two materials.

This method allows for a randomization of the perturbation, which is most realistic and most closely resembles an experimental setup.

This research considers two loading cases: constant strain rate and periodic loading. In the first, a compressive displacement is applied at a constant strain rate, $\dot{\varepsilon}$, to the desired strain amplitude, $\Delta\epsilon$, and then unloaded (Fig. 4.5A). The periodic loading case was administered as a sine curve, loaded in compression first (Fig. 4.5B), given by the following equation:

$$\epsilon(t) = -\Delta\epsilon \sin(\omega t) \tag{4.11}$$

Where $\Delta\epsilon$ is the strain amplitude, and ω is the frequency in radians per second.

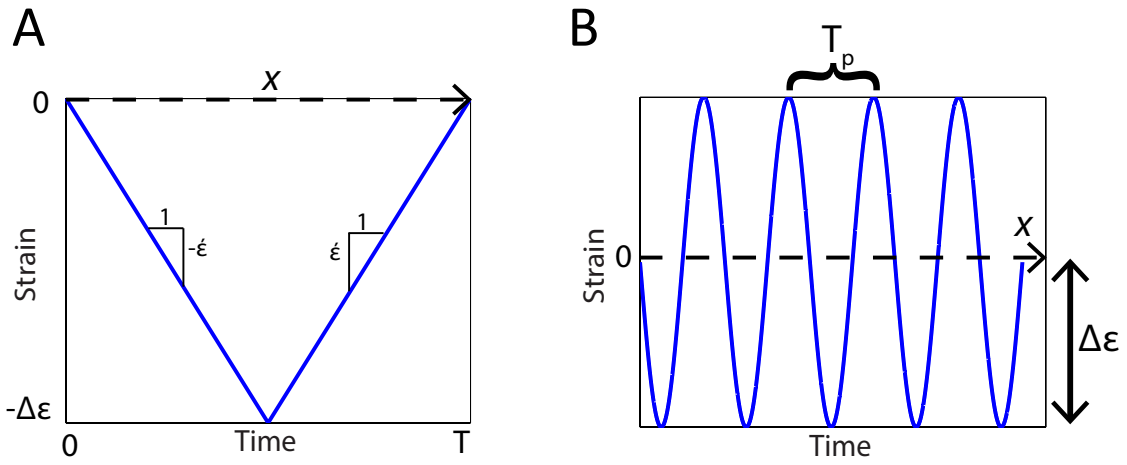

Figure 4.5: A. Constant strain rate loading where $\Delta\epsilon$ is the strain amplitude, $\dot{\epsilon}$ is the strain rate and T is the duration of loading. B. Sinusoidal loading where $\Delta\epsilon$ is the strain amplitude, and T_p is the period.

4.1.5 Meshing

All models are meshed using 4-node bilinear plane strain quadrilateral elements (CPE4RH). Hybrid formulation was used for the mesh elements as is required when modeling nearly incompressible materials [6, 29]. Reduced integration was also employed as this is often advisable when considering problems involving non-linearities

[29]. In the case of linear elements, as was the case here, there is a single integration point at the center of the element as shown in Fig. 4.6A [6]. Reduced integration however is susceptible to numerical errors called hourglassing which is displayed in Fig. 4.6B [6].

Hourglassing is a result of zero-energy modes of deformation. To clarify, Fig. 4.6B, shows that while the element does deform, the point at which the integration occurs (the center) does not experience any strain, thus there is no strain energy. If the mesh is coarse, this hourglassing deformation can propagate through the mesh giving a trivial solution. This numerical error can be corrected through the use of hourglass control and an appropriate mesh density [6].

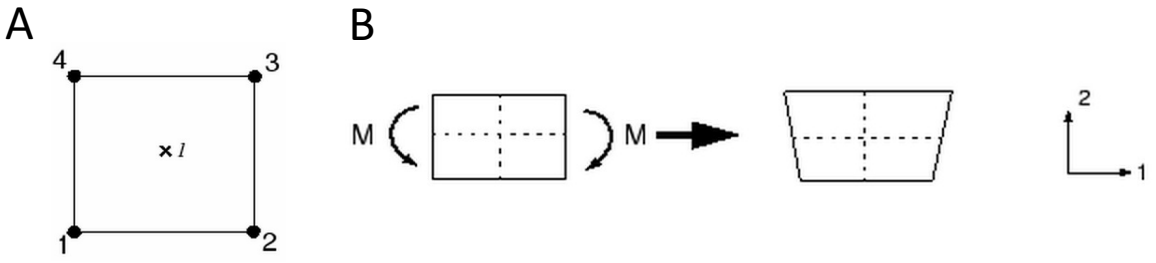

Figure 4.6: A. Linear element with reduced integration B. Hourglassing of reduced integration element [6].

Hourglassing can be controlled in ABAQUS using 2 methods: hourglass stiffness and enhanced control. To understand which had the least effect on the results, several options were compared. After running numerical experiments considering various values for the hourglass stiffness, an hourglass stiffness value of 0.75 was found to give the best results, especially at low strain amplitudes.

When considering how dense the mesh needs to be there are two main factors that must be considered: volume fraction of the stiff material as well as the buckling wavelength. When considering a dilute case (when the volume fraction of the stiff material is small) the composite is subject to buckling in a wavy form. This means that the model is subject to bending. To properly capture this, at least 5 elements

were required across the thickness of a material when the volume fraction was small, with a maximum aspect ratio of 3. Similar results have been found in the literature and previous research for modeling thin structures [3, 6]. Mesh convergence studies were used to verify that a dense enough mesh was used. To aid in deciding an appropriate mesh density, distortion control was also employed. This feature is by default turned on when using hyperelastic materials. Its purpose is to provide a method to stop elements from excessively distorting when the mesh is not very dense and is under compressive loads [6].

4.2 Material models and parameters

Material A was modeled with a neo-Hookean strain energy potential, with a Young's modulus similar to that of steel. Material B was modeled as a standard linear solid. The elastic part was modeled with a neo-Hookean strain energy potential, while the viscoelastic part was modeled using the finite deformation model in ABAQUS based on a Prony series representation. The Prony series data was based on a high loss polyurethane characterized by Sain et. al [33]. The mechanical properties of this material are shown in Fig. 4.7. Table 4.1 details these material parameters and refers to variables commonly used to describe materials. Appendix A provides an overview on the respective parameters that must be inputted into ABAQUS.

Because the theoretical formulae derived in [1] assumes incompressible materials, two values for the Young's modulus and Poisson's ratio for material A were considered: 164.8 GPa (incompressible case used for the theory), 200 GPa (compressible case used for numerical simulations). For the incompressible case, the value of the Young's modulus of material A, E_A, was chosen such that the plane strain modulus, $E_A = E_A/(1-\nu_A^2)$, was equal to its value in the compressible case. Simulations showed that as long as the correct respective Poisson's ratio was used, there is minimal influence on the numerical results (see Fig. 6.3). Material B was modeled to be incompressible

for the numerical simulations.

Table 4.1: Model parameters for material A and material B

Symbol	Description	Value
E_A	Young's modulus (compressible) Young's modulus (incompressible)	200, 000 MPa 164,800 MPa
ν_A	Poisson's ratio (compressible) Poisson's ratio (incompressible)	0.3 0.5
$E_B^{(\infty)}$	Long-term Young's modulus	3.345 MPa
$\nu_B^{(\infty)}$	Long-term Poisson's ratio	0.5
$E_B^{(\alpha)}$	Viscoelastic branch Young's modulus	450MPa
$\nu_B^{(\alpha)}$	Viscoelastic branch poisson ratio	0.5
$\tau_B^{(\alpha)}$	Relaxation time constant	0.15 s

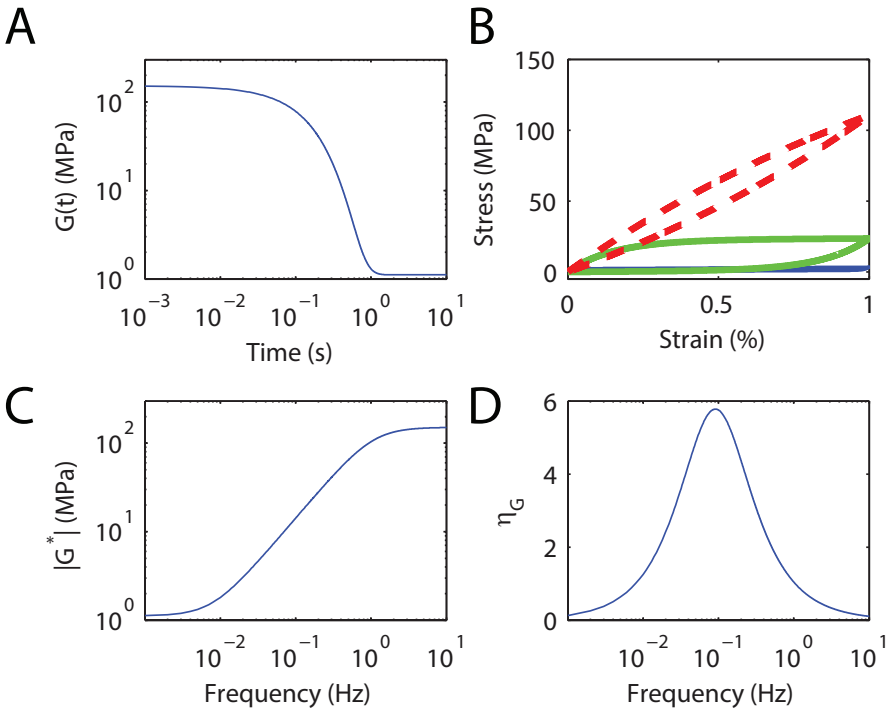

Figure 4.7: Mechanical properties of material B. A. Relaxation shear modulus vs time. B. Shear stress vs shear strain for loading/unloading at a constant shear strain rate of 0.1, 1 and 10%/s. C. Dynamic shear modulus, $|G^*|$, vs frequency. D. Shear loss factor, η_G, vs frequency

4.3 Post processing

To post process the simulations, data must be extracted from the completed ODB (output database) file. This can be done both manually and through the use of Python scripts. After extracting the data, MATLAB was used to plot the appropriate figures. Extracting stress and strain data and analyzing the stress vs strain response provides the information needed to find the strain at which buckling occurs. To analyze the evolution of buckling in the composite the wavenumber spectrum was computed by extracting the X-displacement data of nodes along the left edge of the composite, $U_X(0, y)$.

4.3.1 Computation of the wavenumber spectrum

When periodic boundary conditions are used, the top edge is free to move in the X-direction. Therefore, the composite may deform/buckle with an angle with respect to the Y-axis. Consequently, the derivative of the displacement, denoted here as $\theta(y)$, is periodic with a period H.

$$\theta(y) = \frac{\partial u_X(0, y)}{\partial Y} \tag{4.12}$$

To compute the wavenumber spectrum the Fourier Transform of $\theta(y)$ was calculated:

$$\begin{aligned} \Theta(k) &= \int_{-\infty}^{\infty} \theta(y) e^{-\imath k y} dy \\ &= \int_{0}^{H} \theta(y) e^{-\imath k y} dy \\ &= \mathcal{F}(\theta(y)) \end{aligned}$$

where Θ is a complex number and k is the wavenumber. This was done using MATLAB's FFT algorithm. The absolute value of $\Theta(k)$, $|\Theta(k)|$, was taken to find the wavenumber spectrum.

Chapter 5

Buckling of Elastic Layered Composites

5.1 Critical wavenumber and buckling strain

Parnes and Chiskis [28] derived formulae for the critical buckling strain, ϵ_{cr}, and critical buckling wavelength, L_{cr} for elastic layered composites by modeling the stiff fibres as Euler Bernoulli beams for the plane stress case. The theory assumed that $E_A \gg E_B$ and that the buckling mode is a sinusoid. Alur and Meaud [1] altered the equations for the plane strain case (strain in the out of plane direction is 0). Finite element buckling simulations were used to validate this theory. Buckling is a linear perturbation analysis that requires linear elastic material models. Nonlinear properties as well as properties that are affected by strain rate and time are ignored. Since material B is a viscoelastic material, it is time-dependent. Therefore, two different values for the Young's modulus of material B were considered for the buckling analysis:

1. The long-term Young's modulus, $E_B^{(\infty)}$
2. The instantaneous Young's modulus, $E_B^{(0)} = E_B^{(\infty)} + E_B^{(\alpha)}$

$E_B^{(\infty)}$ and $E_B^{(0)}$ correspond to the lower and upper bounds, respectively, for the time-dependent Young's modulus of material B.

Figs. 5.1A through C show ϵ_{cr} while Figs. 5.1D through F show the nondimensional wavenumber ($\bar{k}_{cr} = Wk_{cr} = (2\pi W)/L_{cr}$, where W is the width of the unit cell) as functions of the volume fraction of material A, ϕ_A. Each column of Fig. 5.1 corresponds to a different stiffness for E_A, decreasing in value from left to right: 200 GPa, 20 GPa and 2 GPa respectively. The simulations and theory match very well for E_A = 200 GPa, however discrepancies between the two are noticeable when E_A = 20 GPa and $E_B = E_B^{(0)}$ ($\frac{E_A}{E_B} \approx 44.1$). In this case the ratio between E_A and E_B is

not big enough for the theory to be a good approximation. For each set of graphs, three different cases can be identified and are examined more closely in Figs. 5.1G through I. These cases were identified as the dilute, transition and non-dilute cases:

1. When $\bar{k}_{cr} \neq 0$ both in the case $E_B = E_B^{(\infty)}$ and $E_B = E_B^{(0)}$ (dilute case)

2. When $\bar{k}_{cr} \neq 0$ if $E_B = E_B^{(0)}$ and $k_{cr} = 0$ if $E_B = E_B^{(\infty)}$ (transition case)

3. When $\bar{k}_{cr} = 0$ both in the case $E_B = E_B^{(\infty)}$ and $E_B = E_B^{(0)}$ (non-dilute case).

The transition case is interesting, as the value for the wavelength actually changes from a finite value to an infinite value, when E_B varies between $E_B^{(0)}$ and $E_B^{(\infty)}$. Fig. 5.2A illustrates the buckling shape in the case $\bar{k}_{cr} = 0$ (which corresponds to $L_{cr} = \infty$, the non-dilute case) while Fig. 5.2B is an example of the buckling shape in the case $\bar{k}_{cr} \neq 0$ (which corresponds to $0 < L_{cr} < \infty$, the dilute case.).

When E_A is fixed, the value of ϵ_{cr} decreases as ϕ_A is increased (Fig. 5.1A through C). For any given value of ϕ_A, ϵ_{cr} is higher in the case $E_B = E_B^{(0)}$ than in the case $E_B = E_B^{(\infty)}$, which indicates that increasing E_B tends to increase the buckling strain of the composite. However, when ϕ_A is fixed, the value of ϵ_{cr} increases as E_A is decreased. This shows that ϵ_{cr} is a function of the ratio, $\frac{E_A}{E_B}$, of the two materials.

Using the theory from [1], ranges for each case, which depend on both E_A and ϕ_A, can be found and are shown in Fig. 5.3. This was done by finding the volume fraction at which the composite transitions from the dilute to transition and transition to non-dilute cases for various values of E_A.

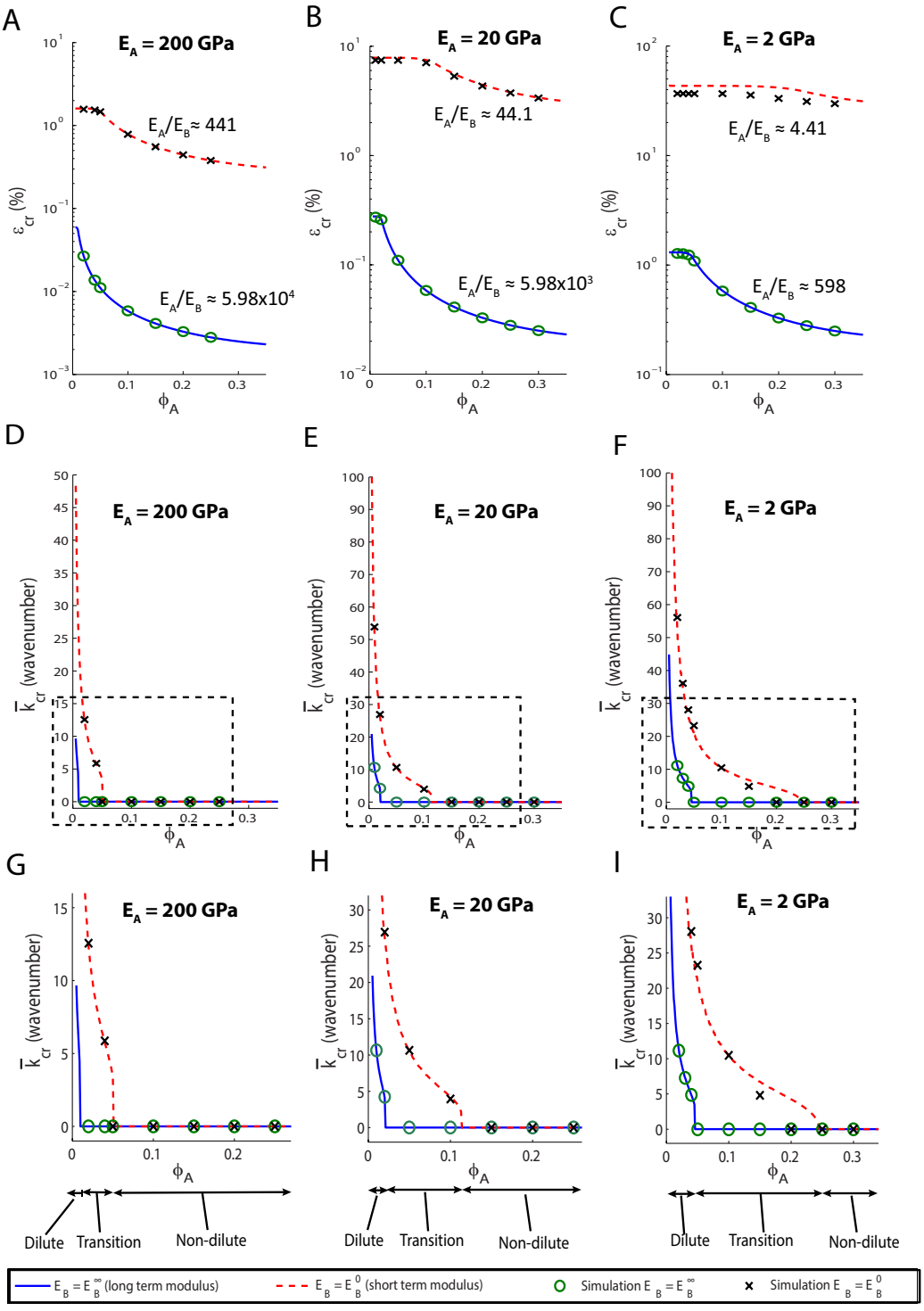

Figure 5.1: Dependence of the buckling wavenumber and critical strain on the volume fraction and Young's modulus of material A and the Young's modulus of material B. Critical strain vs ϕ_A for long and short term E_B for A. E_A=200GPa B. E_A=20GPa C. E_A=2GPa. Non-dimensional wavenumber, $\bar{k}_{cr}$, vs ϕ_A for long and short term E_B for D. E_A=200GPa E. E_A=20GPa F. E_A=2GPa. Zoomed in view for $\bar{k}_{cr}$, vs ϕ_A for showing various cases for G. E_A=200GPa H. E_A=20GPa I. E_A=2GPa.

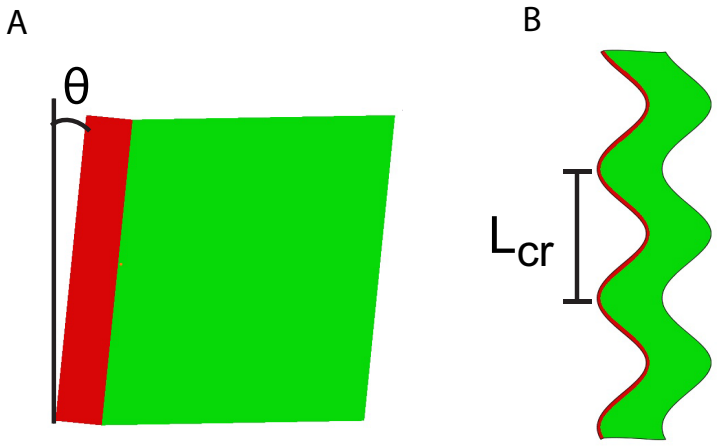

Figure 5.2: A. Buckling shape with infinite wavelength ($\bar{k}_{cr}$=0) for non-dilute composites. The layers deform but remain straight. The amplitude of the buckling shape is parameterized by the angle θ. B. Buckling shape with finite wavelength, L_{cr}, for dilute composites.

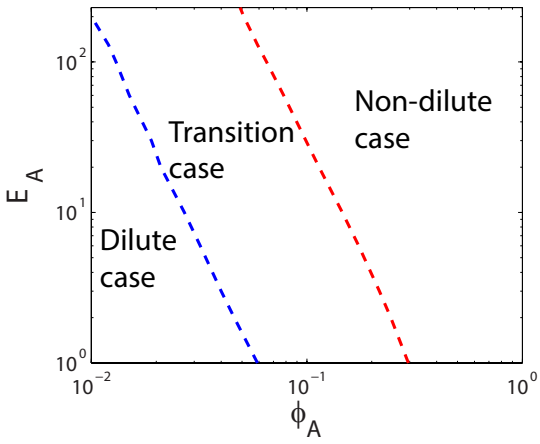

Figure 5.3: Ranges for each case (dilute, transition and non-dilute) based on E_A and ϕ_A

5.2 Finite height consideration

Buckling analysis, conducted for models of finite height, but with an infinite number of layers, showed that the height of the composite can have an effect on the response. Fig. 5.4 shows the critical buckling strain as a function of the height for the upper and lower bounds of E_B. Fig. 5.4A shows this for E_A = 200 GPa and Fig. 5.4B

for $E_A = 2$ GPa. Both are shown for the non-dilute case ($\phi_A = 25\%$) because the buckling mode ($\bar{k}_{cr} = 0$) does not depend on H for a non-dilute model with periodic boundary conditions ($\frac{H}{W} = 1$). For all cases, as long as the ratio $\frac{E_A}{E_B}$ is high enough ($\frac{E_A}{E_B} \gtrsim 50$), as the height of the model increases, the critical buckling strain converges to the theoretical value for a model of infinite size. The infinite size model can identify the critical buckling strain as long as $\frac{H}{W} \geq 50$.

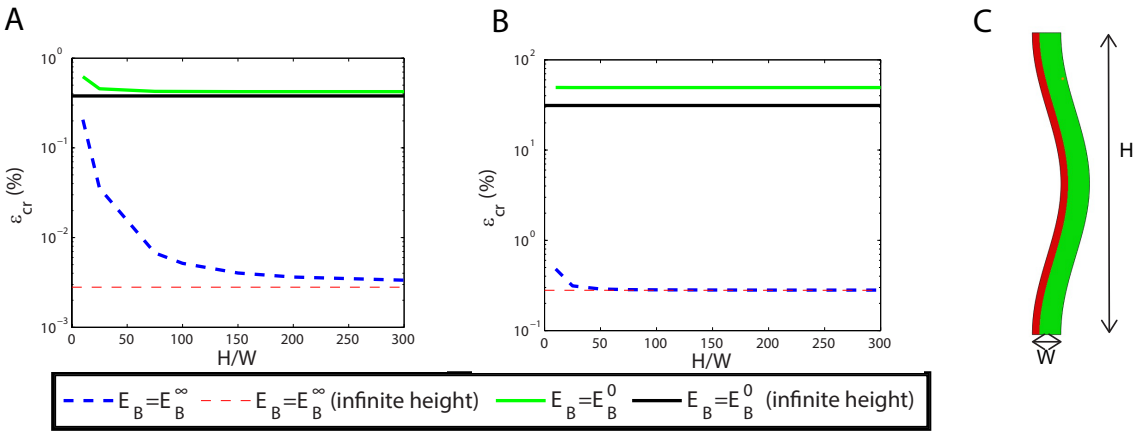

Figure 5.4: Critical buckling strain vs height for $E_B = E_B^{(\infty)}$ and $E_B = E_B^{(0)}$ for A. E_A = 200 GPa B. $E_A = 2$ GPa. . Horizontal lines correspond to infinite height FEM simulated results. C. Buckling shape for finite height boundary conditions.

5.3 Conclusions

These numerical results give important qualitative information regarding the finite deformation response of viscoelastic layered composites. The relaxation modulus of a viscoelastic material decreases as a function of time (see Fig. 4.7A). If the viscoelastic composite is loaded in compression at a constant strain rate, the composite is expected to buckle with an infinite wavelength provided that ϕ_A is in the non-dilute region. If ϕ_A is in the transition region, the mode of deformation might progressively change from a small finite wavelength to a larger finite or possibly infinite wavelength (depending on the strain rate). If ϕ_A is in the dilute region, the composite is expected to deform with a finite buckling wavelength (that might increase over time). Since

the buckling strain is higher in the case $E_B = E_B^{(0)}$ than in the case $E_B = E_B^{(\infty)}$ (Fig. 5.1A through C), the buckling strain is expected to be higher at high strain rates than at low strain rates in the case of a viscoelastic composite.

Chapter 6

Constant Strain Rate Finite Deformation Analysis

To understand the mechanics of parallel plane layered viscoelastic composites, finite deformation analysis was performed. Studying the response to a constant loading rate provides the necessary information to characterize the evolution of buckling.

6.1 Viscoelastic constituents

Expanding upon equations derived by Rudykh and Boyce [31] for elastic layered composites in the non-dilute case, Alur and Meaud [1] extended the equations to characterize the finite deformation response of non-dilute (infinite buckling wavelength) viscoelastic layered composites with the following assumptions:

1. Incompressible materials

2. Infinite buckling wavelength

After validation using finite element simulations, the theory was used to understand the response for the non-dilute case. On the other hand, both the transition and dilute cases were examined using finite element simulations. The model parameters chosen for analysis for each case are shown in Table 6.1. These values are also represented in Fig. 6.1.

Table 6.1: Parameters for each case

Case	**Volume fraction** ϕ_A	E_A
Dilute	2%	2 GPa
Transition	15%	2 GPa
Non-Dilute	25%	200 GPa

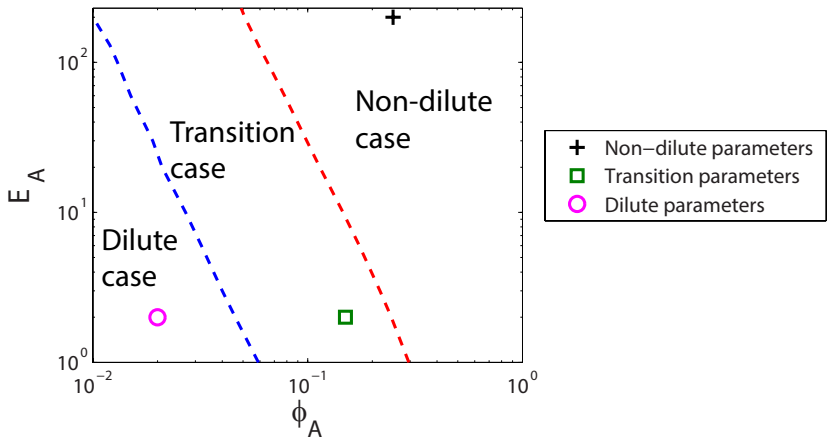

Figure 6.1: Ranges for each case (dilute, transition and non-dilute) based on E_A and ϕ_A shown with points used for simulations.

6.1.1 Validation of theory for non-dilute composites

The finite deformation theory for viscoelastic layered composites [1] was validated by comparison to finite element simulations. The stress vs. strain response was plotted for small and large initial angles (1 and 45 degrees) for a broad range of strain rates (0.1 to $10\%/s$). As shown in Fig. 6.2, the theory (shown in solid lines) and the simulated response (dotted lines) match exactly. Thus, the finite deformation theory was used with confidence for all the results for infinite size non-dilute composites with incompressible constituents.

6.1.2 Effect of compressibility

The finite deformation theory derived in [1] assumes that the two constituents are incompressible. While this assumption is a good approximation for polymers and rubber-like materials, it does not hold for materials like steel. Fig. 6.3 compares the stress vs. strain response for two different values for the Poisson's ratio of material A ($\nu_A = 0.3$ and $\nu_A = 0.5$). The Young's modulus in each instance is such that the plane strain modulus is the same ($i.e\ \frac{E_A}{1-\nu^2}$ is a constant). Barely any difference can be

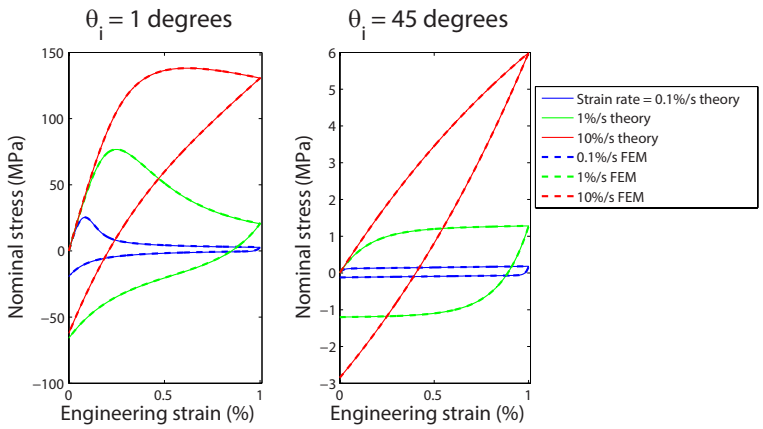

Figure 6.2: Comparison between the finite deformation theory and finite deformation finite element simulations for viscoelastic composites. The theory is shown in solid lines; simulations, shown in dashed lines, are indistinguishable from the theory for different values of the initial angle, θ_0, and a wide range of strain rates.

discerned between the two responses which indicates that assuming incompressibility does not affect the numerical results as long as the change in the effective plane strain stiffness is accounted for accordingly.

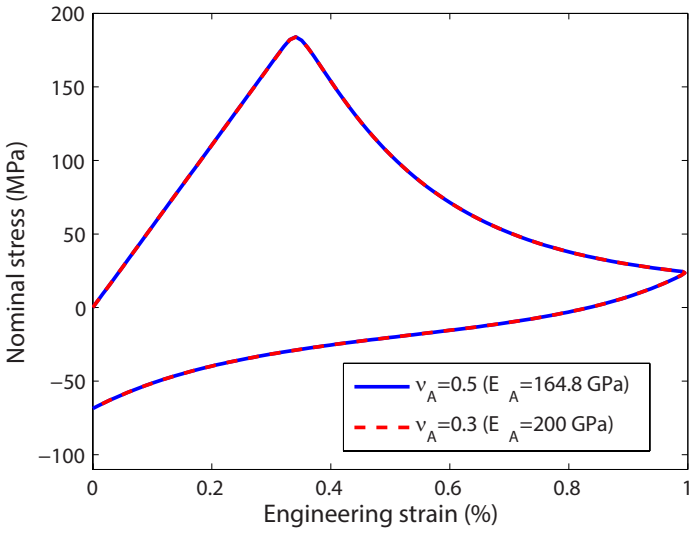

Figure 6.3: Stress vs. strain response for the incompressible ($\nu_A = 0.5$) and compressible cases ($\nu_A = 0.3$). For the compressive case, the results were obtained using finite element simulations.

6.1.3 Adding the appropriate imperfection

Simulations for the non-dilute case were done by applying an imperfection as a scaling of the first buckling mode, characterized by an infinite wavelength. Various scaling factors were compared to find the one with the least effect on the response. Fig. 6.4 shows the scaling factor's effect on the response, shown for a composite consisting of elastic constituents. Lowering the scaling factor of the imperfection results in a response more similar to one without any imperfection. Based on this analysis, a scaling factor of 1×10^{-4} was chosen.

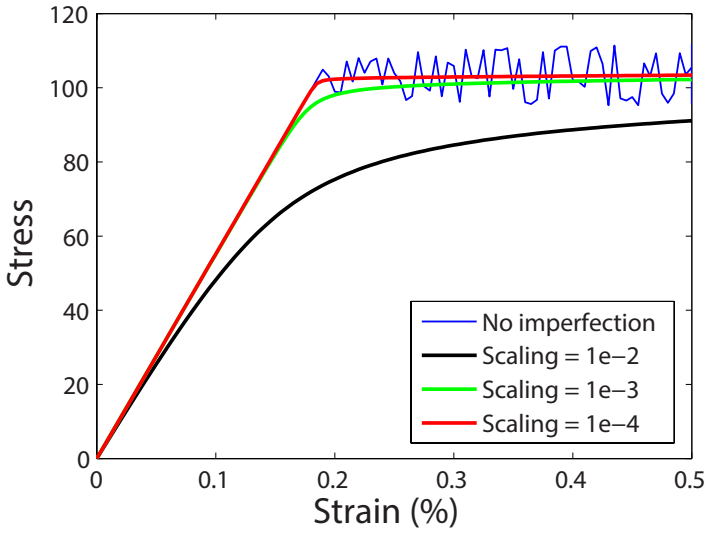

Figure 6.4: Stress-strain response for the non-dilute case comparing various imperfection scalings.

For dilute and transition case simulations, random imperfections were applied directly to the model to simulate a realistic situation. Matlab's random number generator was used to apply small perturbations to both vertical edges as well as at the interface between the two materials with a uniform distribution in the following manner:

$$X_i|_{With\ Imperfection} = X_i|_{Without\ Imperfection} + R_i W \tag{6.1}$$

Where X_i refers to the horizontal coordinate of node i, R_i is the perturbation that is applied to node i within range R (see Fig. 6.5) and W is the width of the unit cell.

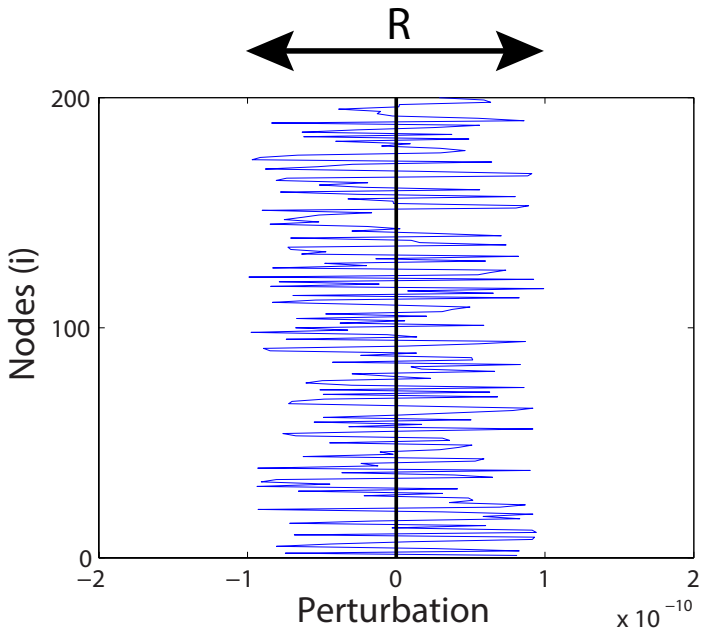

Figure 6.5: Example of an imperfection of range R on a vertical edge

The stress vs strain responses for infinite buckling wavelength models (transition case with a low strain rate) with various imperfections were compared with the response for a composite which did not contain any imperfections but had a very small angle between the layer and loading directions. This ensured comparison to an infinite buckling wavelength model. While the angle of the model does affect the response, the angle chosen here (1×10^{-8} degrees) was small enough to have a very minor affect. Fig. 6.6 shows the stress vs strain response for various imperfections. As the imperfection size decreases, the critical buckling strain increases and converges towards the value for the angled model. Closer inspection shows that imperfections 4 and 5 have very similar responses, and is most likely due to the fact that the random number generator chooses numbers over a range of values. This means that the difference between two consecutive imperfections may indeed be very similar if one is on the upper end and the other on the lower end of their respective ranges. Details for each

imperfection are shown in Table 6.2. As long as the perturbations are on the order of magnitude of 1×10^{-10} (Imperfection 6) the imperfection will not alter the response. Thus, this imperfection size was chosen for all subsequent results shown.

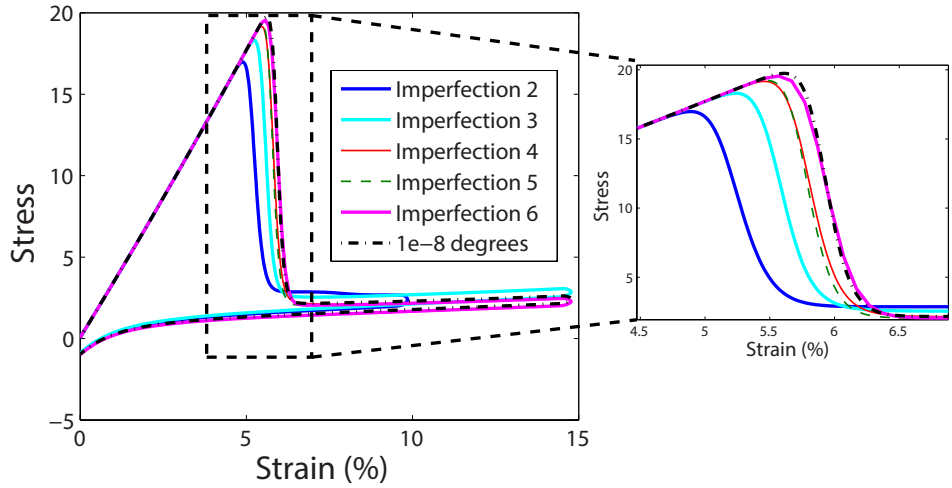

Figure 6.6: Stress-strain response for the dilute case comparing models with various imperfections compared to a model with a small angle but without any imperfections.

Table 6.2: Details for various imperfections considered.

Imperfection	**Range (R) for perturbation**
Imperfection 2	$\pm 1 \times 10^{-6}$
Imperfection 3	$\pm 1 \times 10^{-7}$
Imperfection 4	$\pm 1 \times 10^{-8}$
Imperfection 5	$\pm 1 \times 10^{-9}$
Imperfection 6	$\pm 1 \times 10^{-10}$

6.1.4 Effect of strain rate

The critical buckling strain for a viscoelastic composite depends on the strain rate. This dependence is investigated in Fig. 6.7 which shows a monotonic relationship between the the critical buckling strain and the strain rate. Fig. 6.7A considers the non-dilute case, Fig. 6.7B the dilute case and Fig 6.7C the transition case. For all cases, at low strain rates, the curve tends to converge to the value obtained using a linear buckling theory analysis when $E_B = E_B^{(\infty)}$, the long term Young's modulus for

material B. For the non-dilute case, at a high strain rate, the curve tends to converge to the value obtained using a linear buckling theory analysis when $E_B = E_B^{(0)}$, the short term Young's modulus for material B. Note that a small difference can be observed between the value at large strain rate and the theoretical linear buckling critical strain for $E_B = E_B^{(0)}$. This difference might be due to the fact that the buckling analysis is a linear theory that neglects nonlinear effects. For the dilute and transition cases, at high strain rates, these curves converge to a value that is close to what was obtained using linear buckling finite element analysis when $E_B = E_B^{(0)}$. For the dilute and transition cases considered, the ratio of $\frac{E_A}{E_B}$ is not high enough for the theory to be a good approximation (see Figs. 5.1B and C).

The dependence of the critical wavenumber, $\bar{k}_{cr}$, on the strain rate is investigated in Figs. 6.8A and B, for the dilute and transition cases respectively. At low strain rates the curve converges towards the value obtained using linear buckling simulations when $E_B = E_B^{(\infty)}$. As the strain rate increases, the relationship is monotonic in both cases. For the dilute case, if even higher strain rates were simulated, the curve would likely converge towards the value obtained for linear buckling simulations when $E_B = E_B^{(0)}$. In the transition case the value for $\bar{k}_{cr}$ actually exceeds the value attained from buckling simulations when $E_B = E_B^{(0)}$. This result is unexpected, and could be a result of the height chosen. The wavenumber that was calculated is one of the possible values for the height for this simulation.

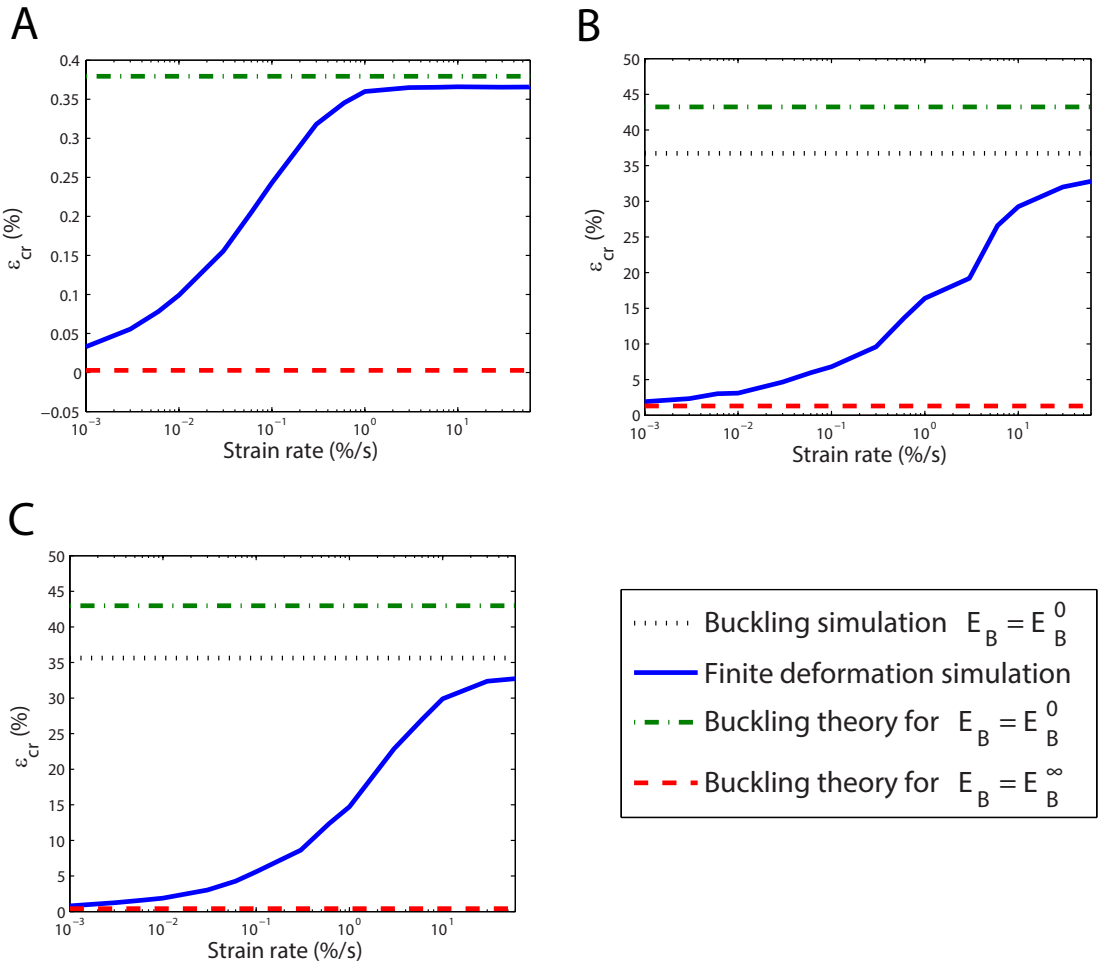

Figure 6.7: Critical buckling strain vs strain rate for A. Non-dilute case B. Dilute case C. Transition case.

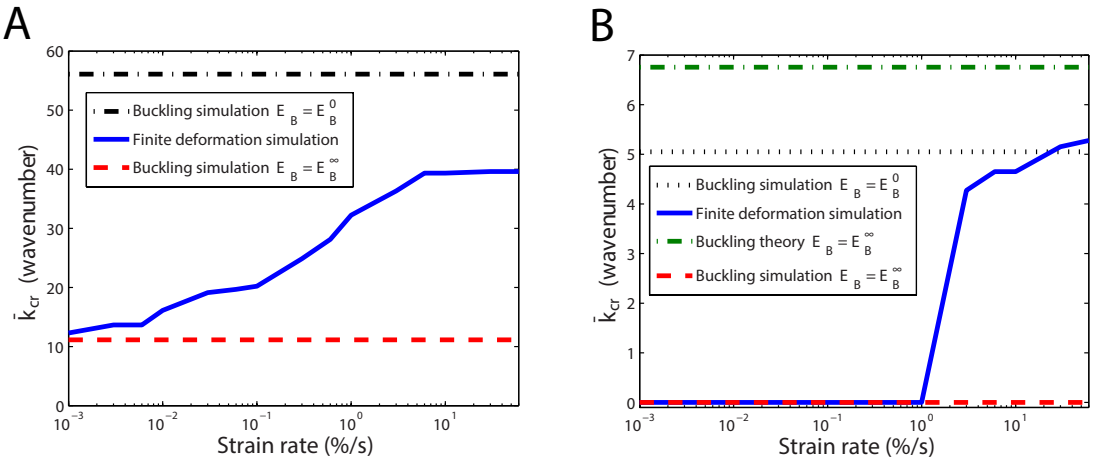

Figure 6.8: Critical wavenumber vs strain rate shown for the A. Dilute case and B. Transition case.

6.1.5 Finite height consideration

Models of finite height were also considered for the finite deformation case. Fig. 6.9 shows the stress vs strain response for non-dilute composites attained through finite deformation simulations for composites of a finite height, compared to that of infinite height attained from the finite deformation theory from [1]. There is a small difference between the critical strain as well as the stress vs strain responses: the critical strains and stresses are slightly higher in the finite height case. This is a result of the boundary conditions. The horizontal displacement is fixed on the top and bottom boundaries for the finite height simulations, which constrains the mode of deformation. However, these results do demonstrate that the finite deformation model for composites of infinite height can capture the stress vs strain response of composites of finite height as long as $H/W \geq 50$.

Finite height simulations for the dilute case were not completed and are not shown in these results. Similar results to the non-dilute case are expected.

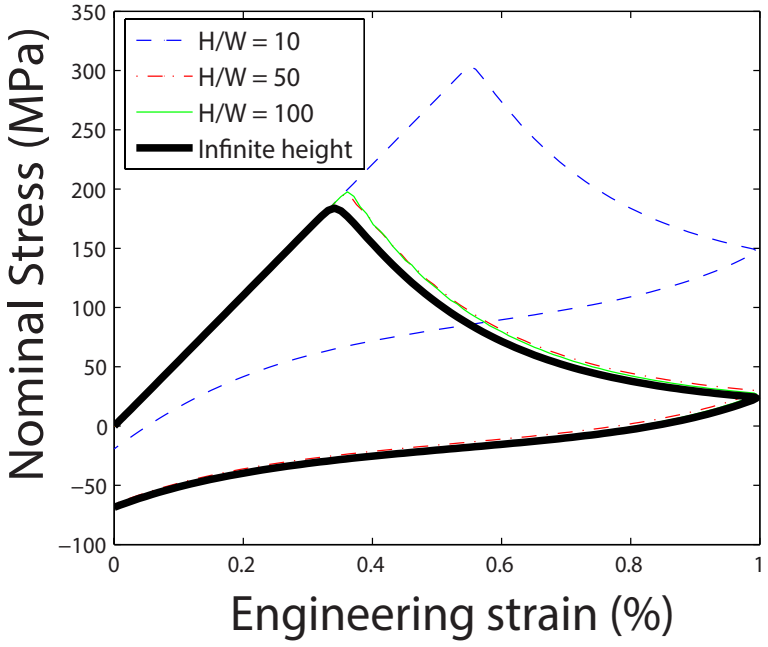

Figure 6.9: Stress vs strain response for various heights compared to that of infinite height.

6.1.6 Evolution of buckling

The mode and evolution of buckling in viscoelastic layered composites is dependent on two main things:

1. Which case the composite falls under: dilute, transition or non-dilute. This is dependent on E_A and ϕ_A (Fig. 5.3).

2. The strain rate.

For all three cases, the response was studied at both low and high strain rates. Looking at the stress vs strain response gives a clear picture on when buckling occurs, while looking at how the wavelength changes over time gives a clear idea of how the composite is buckling. Figs. 6.10, 6.11 and 6.12 show these figures for the non-dilute, dilute and transition cases respectively. The left column represents the response for low strain rate while the right for high strain rate. The first figure in each column is the respective stress vs strain responses including the post buckling regime. The next figure is the graph for the nondimensional wavenumber spectrum vs the normalized time ($\bar{t} = \frac{t}{T}$ where T is the duration of the simulation). At each point $(\bar{t}, \bar{k})$, the color corresponds to the normalized amplitude of the mode of wavenumber $\bar{k}$ at time $\bar{t}$. The amplitude is normalized with respect to the maximum magnitude of the wavenumber throughout the entire response. The black line corresponds to the maximum wavenumber at each time. The final figure is the wavenumber spectrum of the response when the composite buckles. The wavenumber spectrum when unloading occurs is also included in the same figure when the composite buckles with a finite wavenumber. The vertical dashed lines correspond to the wavenumber computed from the linear buckling analysis corresponding to the two bounds for E_B (low strain rate: $E_B = E_B^{(\infty)}$; high strain rate: $E_B = E_B^{(0)}$). Examining Figs. A and B between all three figures shows that the critical buckling strain is higher for higher strain rates regardless of which case is considered.

The non-dilute case was defined such that the composite buckles with an infinite wavelength ($\bar{k} = 0$). Fig. 6.10 shows that regardless of the strain rate the composite buckles with an infinite wavelength.

For the dilute case, when the strain rate is low, the composite buckles at a finite wavenumber that decreases as a function of time (Fig. 6.11C). The wavenumber spectrum in Fig. 6.11E shows that the critical buckling wavenumber, $\bar{k}_{cr}$, gets closer to the wavenumber that was found from linear buckling analysis when $E_B = E_B^{(\infty)}$ (Fig. 5.1I) with time. At a high strain rate, the composite buckles with a finite wavenumber that does not change with time (Fig. 6.11D). One peak is observed near the wavenumber found from linear buckling analysis when $E_B = E_B^{(0)}$; however, the most dominate wavenumber is slightly lower. This shows that even with this strain rate, stress relaxation in the polymer has influenced the response. With a higher strain rate the most dominant wavenumber would be very close to the wavenumber found from linear buckling analysis.

For the transition case, at low strain rates the composite buckles with a wavenumber of zero (Figs. 6.12C and E), which corresponds to the wavenumber found from linear buckling analysis when $E_B = E_B^{(\infty)}$ (Fig. 5.1I). At high strain rates however the composites buckles with a finite wavenumber. The wavenumber spectrum in Fig. 6.12F shows that the wavenumber with the highest magnitude is close to the wavenumber found from linear buckling analysis when $E_B = E_B^{(0)}$. Figs. 6.12D and F show three distinct prominent wavenumbers all of different magnitudes. This is due to harmonic distortion, which occurs at high strain rates (also seen in Figs. 6.11D and F). These peaks approximately occur at integer multiples of the critical buckling wavenumber: $\bar{k}_{cr}$, $2\bar{k}_{cr}$, $3\bar{k}_{cr}$. Fig. 6.13A shows the amplitude ($|\Theta(k)|$) of each of these wavenumbers as a function of time, while Fig. 6.13B shows how these wavenumbers grow over time ($\frac{d|\Theta(k)|}{dt}$). They increase rapidly beginning just before $\bar{t}_{cr}$, at which point the growth rate decreases. The magnitude begins to converge to a value and

then decreases. It is difficult to understand the growth of these wavenumbers since unloading occurs. Therefore, it helps to also look at a similar loading case in which the composite is loaded to a certain strain, and then held for a period of time.

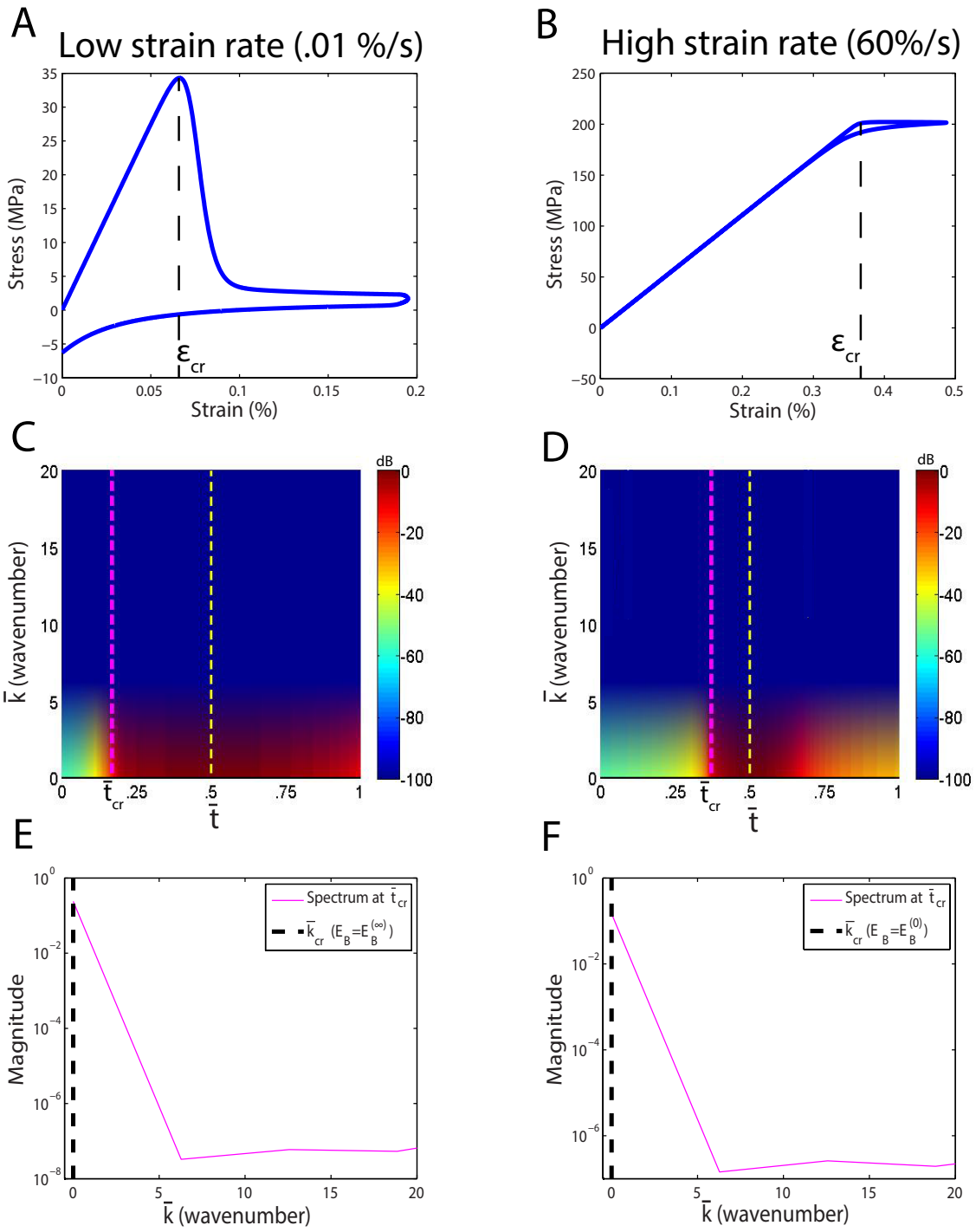

Figure 6.10: Modes and postbuckling for the non-dilute volume fraction case. Stress vs strain response for A. low strain rate B. high strain rate. Nondimensional wavenumber spectrum vs normalized time for C. low strain rate D. high strain rate. Dark black line refers to the maximum wavenumber at any given time. Nondimensional wavenumber spectrum at buckling for E. low strain rate F. high strain rate. Dashed black lines refer to buckling wavenumbers attained from linear buckling analysis.

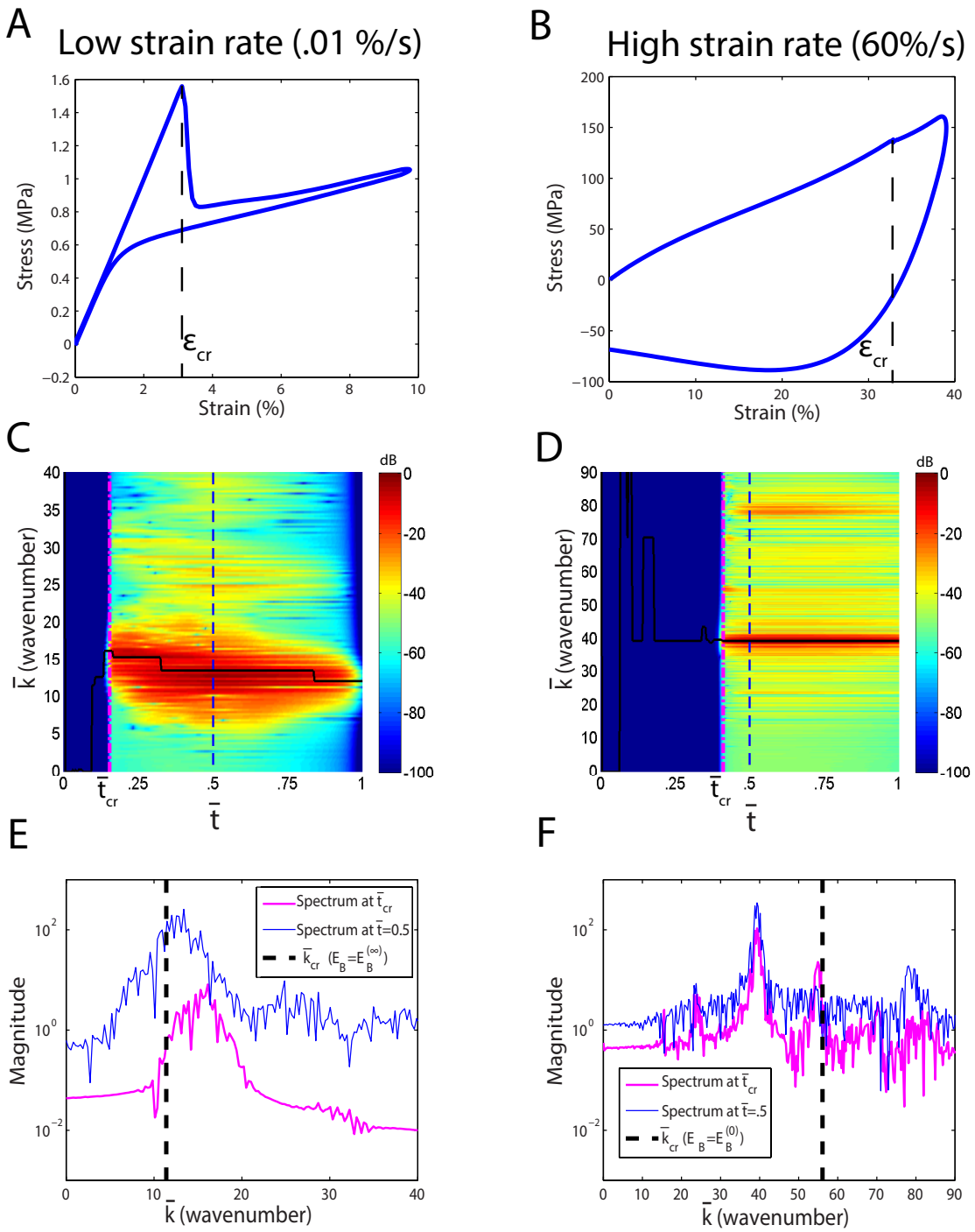

Figure 6.11: Modes and postbuckling for the dilute volume fraction case. Stress vs strain response for A. low strain rate B. high strain rate. Nondimensional wavenumber spectrum vs normalized time for C. low strain rate D. high strain rate. Dark black line refers to the maximum wavenumber at any given time. Nondimensional wavenumber spectrum at buckling and unloading for E. low strain rate F. high strain rate. Dashed black lines refer to buckling wavenumbers attained from linear buckling analysis.

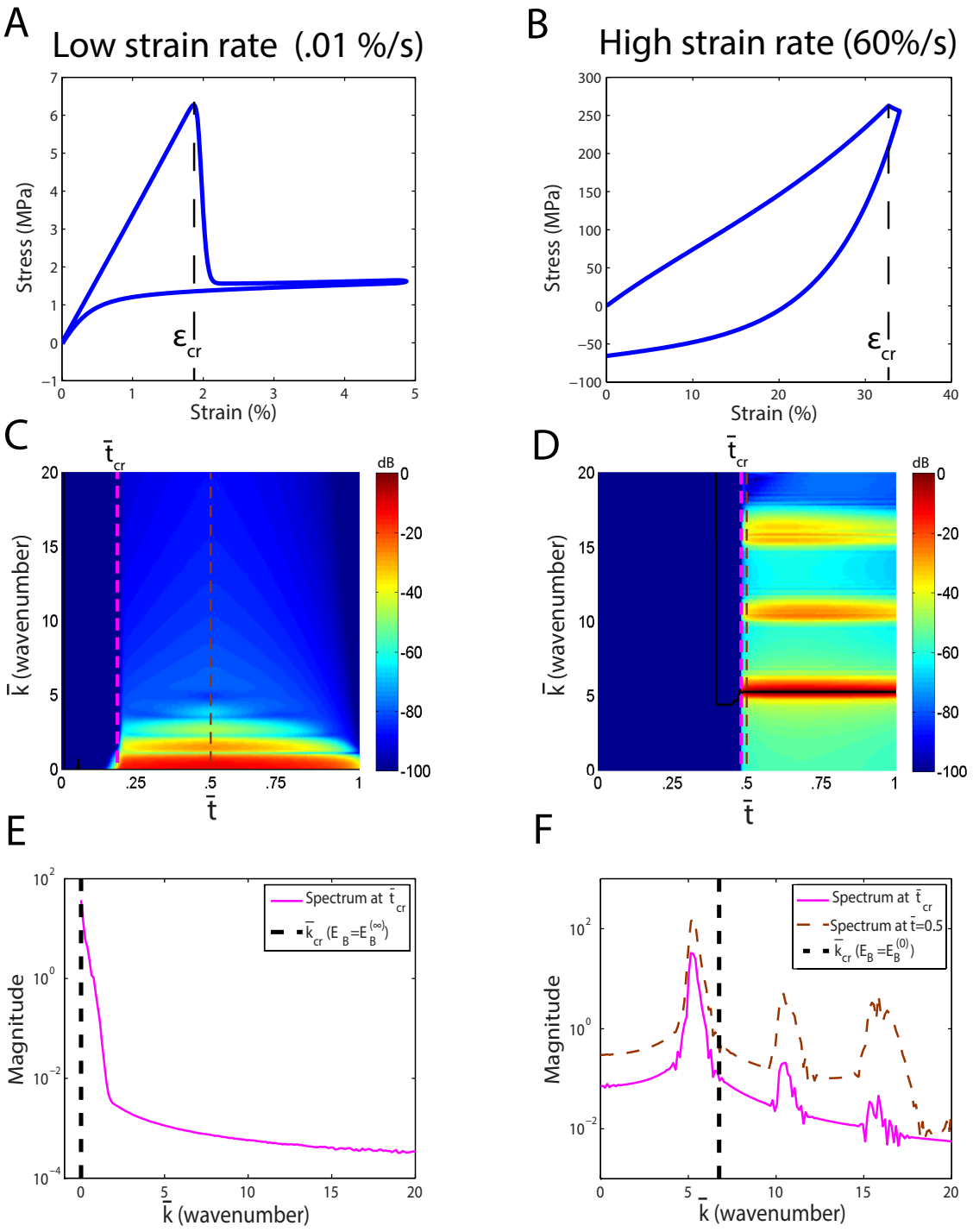

Figure 6.12: Modes and postbuckling for the transition volume fraction case. Stress vs strain response for A. low strain rate B. high strain rate. Nondimensional wavenumber spectrum vs normalized time for C. low strain rate D. high strain rate. Dark black line refers to the maximum wavenumber at any given time. Nondimensional wavenumber spectrum at buckling for E. low strain rate F. high strain rate (unloading shown as well). Dashed black lines refer to buckling wavenumbers attained from linear buckling analysis.

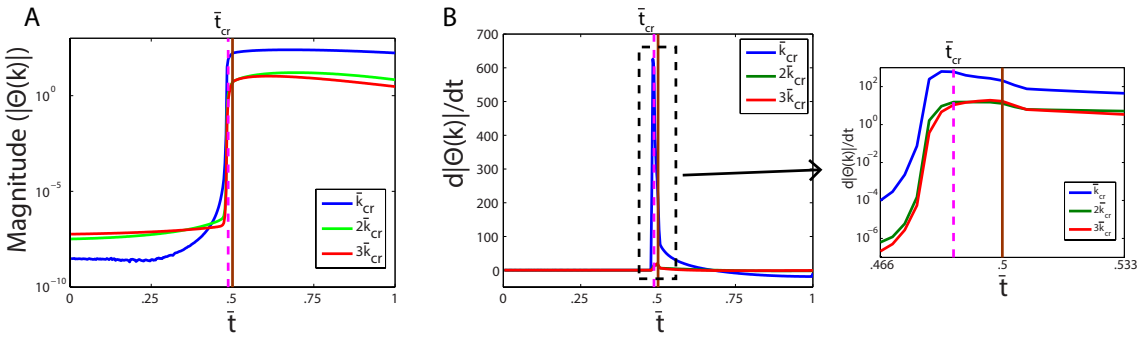

Figure 6.13: A. Magnitude of the wavenumbers that arise from harmonic distortion as a function of time for the transition case. B. Growth rate of the magnitude of these wavenumber shown in log scale.

6.1.7 Holding the strain amplitude constant

Applying a constant strain over a period of time provides some more insight into the finite deformation mechanics. Fig. 6.14 shows this for the transition case. When the strain is held constant, there is stress relaxation (Fig. 6.14A and B) in the polymer and the change in the buckling mode is very apparent. The strain was applied at a constant rate until time $\bar{t}_h$ and then held constant. The strain at $\bar{t}_h$ corresponds to a strain just under ϵ_{cr} (just before buckling). A brief period of time passes as the polymer relaxes and then buckles at time $\bar{t}_{cr}$ with a finite wavenumber which decreases towards zero (Fig. 6.14C). Fig. 6.14D shows that the dominant wavenumber at $\bar{t}_h$ and $\bar{t}_{cr}$ are the same, but is several magnitudes larger at $\bar{t}_{cr}$. As time increases, the value of the most dominant wavenumber converges to 0. While not as clear, there is harmonic distortion in this response as well. Unlike before, the most dominant wavenumber changes as a function of time, so instead of looking at discrete wavenumbers a range of wavenumbers was considered. The range considered is from $\bar{k} = 1.5$ to $\bar{k} = 8$, shown with vertical dashed lines in Fig. 6.14D. These values were chosen such that it encompassed the entire width of the peak at $\bar{t}_{cr}$. The root mean square value of this range was taken to find the average magnitude of the wavy mode of deformation. Fig. 6.15 shows the growth of this value compared with the growth of $\bar{k} = 0$. Initially both

are increasing but the wavy mode dominates. The wavy mode eventually converges to a value and the begins decreasing. While this happens, the 0 wavenumber continues to increase in magnitude and eventually dominates. As the polymer relaxes, the magnitude of the 0 wavenumber converges to a value.

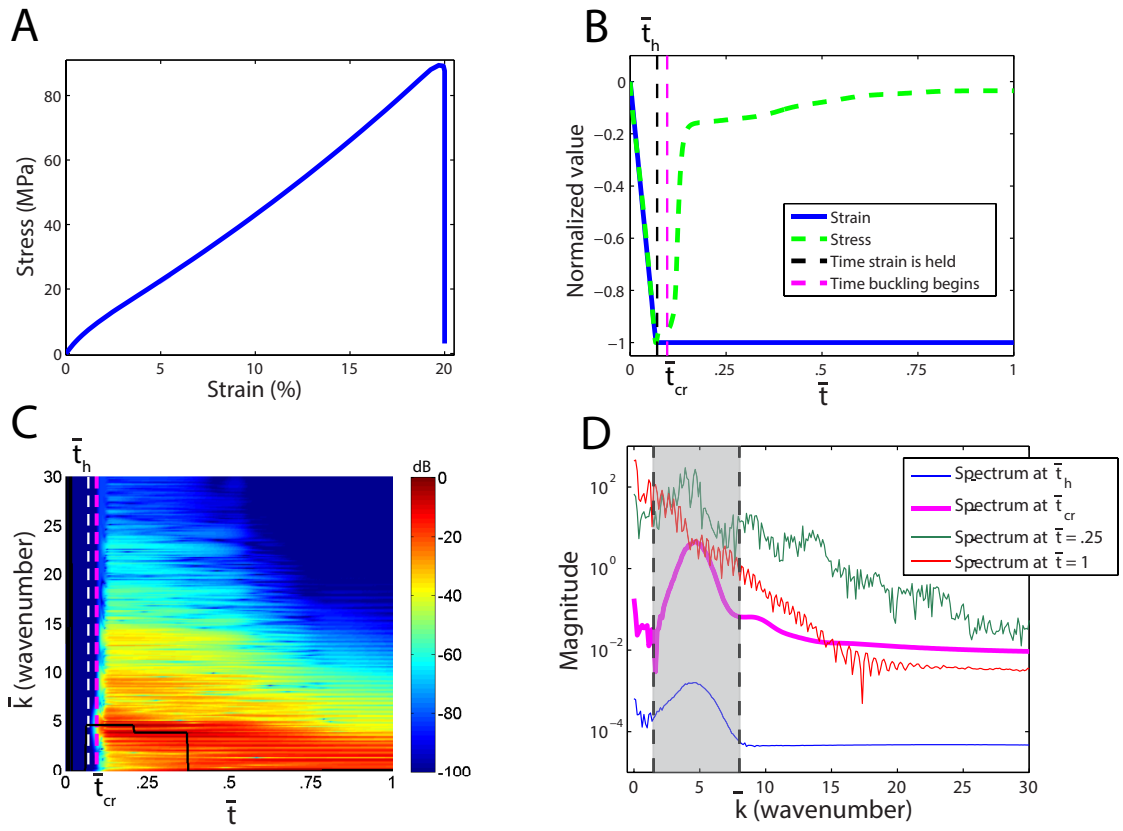

Figure 6.14: Modes and postbuckling for the transition volume fraction case when the strain is held constant. A. Stress vs strain response B. Normalized stress and strain curves vs time. C. Wavenumber spectrum vs time. Dark black line refers to the maximum wavenumber at any given time. D. Wavenumber spectrum at various times. Wavenumbers within the shaded region were considered when calculating the RMS value.

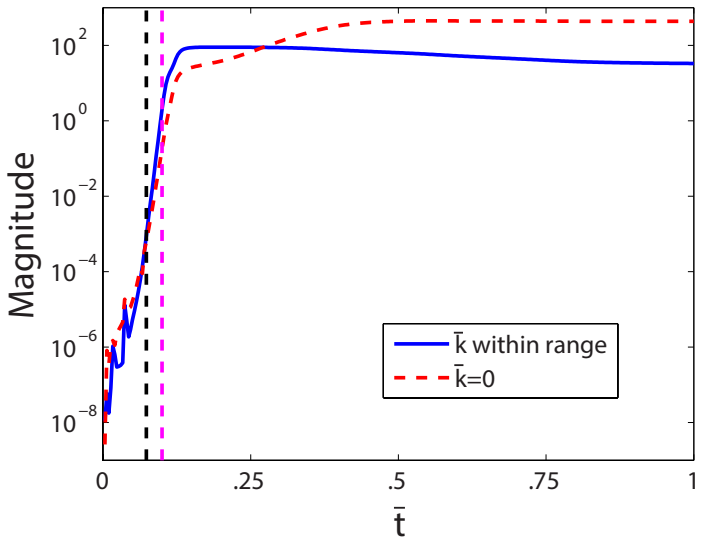

Figure 6.15: Magnitude of the wavenumbers that arise from harmonic distortion as a function of time for the transition case when strain is held constant.

6.1.8 Conclusions

Using the theory from [1] and finite element simulations showed that the finite deformation response of layered composites are consistent with the conclusions gathered from linear buckling analysis. The finite deformation mechanics of viscoelastic parallel plane layered composites are dependent on which case they fall under (dilute, transition, non-dilute) and on the strain rate. If within the non-dilute region, the composite will always buckle with an infinite wavelength. If within the dilute region, the composite will buckle with a finite wavelength that depends on the strain rate. If within the transition region, the composite may buckle with either a finite or infinite wavelength depending on the strain rate. In both the dilute and transition cases the critical buckling wavenumber is within the bounds specified by linear buckling analysis for the long and short term moduli of material B. At high strain rates, harmonic distortion is evident in these cases at approximately integer multiples of $\bar{k}_{cr}$. With time the amplitude of these wavenumbers slightly decreases.

6.2 Elastic constituents

Examining the response of elastic parallel plane layered composites provides more insight into the finite deformation mechanics of viscoelastic parallel plane layered composites. Fig. 6.16 shows the finite deformation response and buckling modes of an elastic composite. Shown here for the transition case with $E_B = E_B^{(0)}$, it is expected to buckle with a finite wavenumber. The peaks seen in the wavenumber spectrum in Fig. 6.16C are very defined, and show that it does indeed buckle close to the same wavenumber that was found from linear buckling simulations. Once the strain exceeds ϵ_{cr}, harmonic distortion is observed at wavenumbers which are approximately integer multiples of $\bar{k}_{cr}$. Unlike the viscoelastic case, these wavenumbers immediately decrease once unloading occurs (Fig. 6.17).

6.2.1 Conclusions

The finite deformation response of an elastic composite results in very defined buckling modes/wavenumbers. Comparing Figs. 6.16B and C with the wavenumber spectrums from the response of viscoelastic composites (Figs. 6.10 through 6.12) shows that viscoelasticity allows the composite to buckle with a range of wavenumbers. Even at high strain rates the peaks in the wavenumber spectrums for viscoelastic composites span a range of wavenumbers. Because of continuous stress relaxation in the polymer, these ranges vary with time.

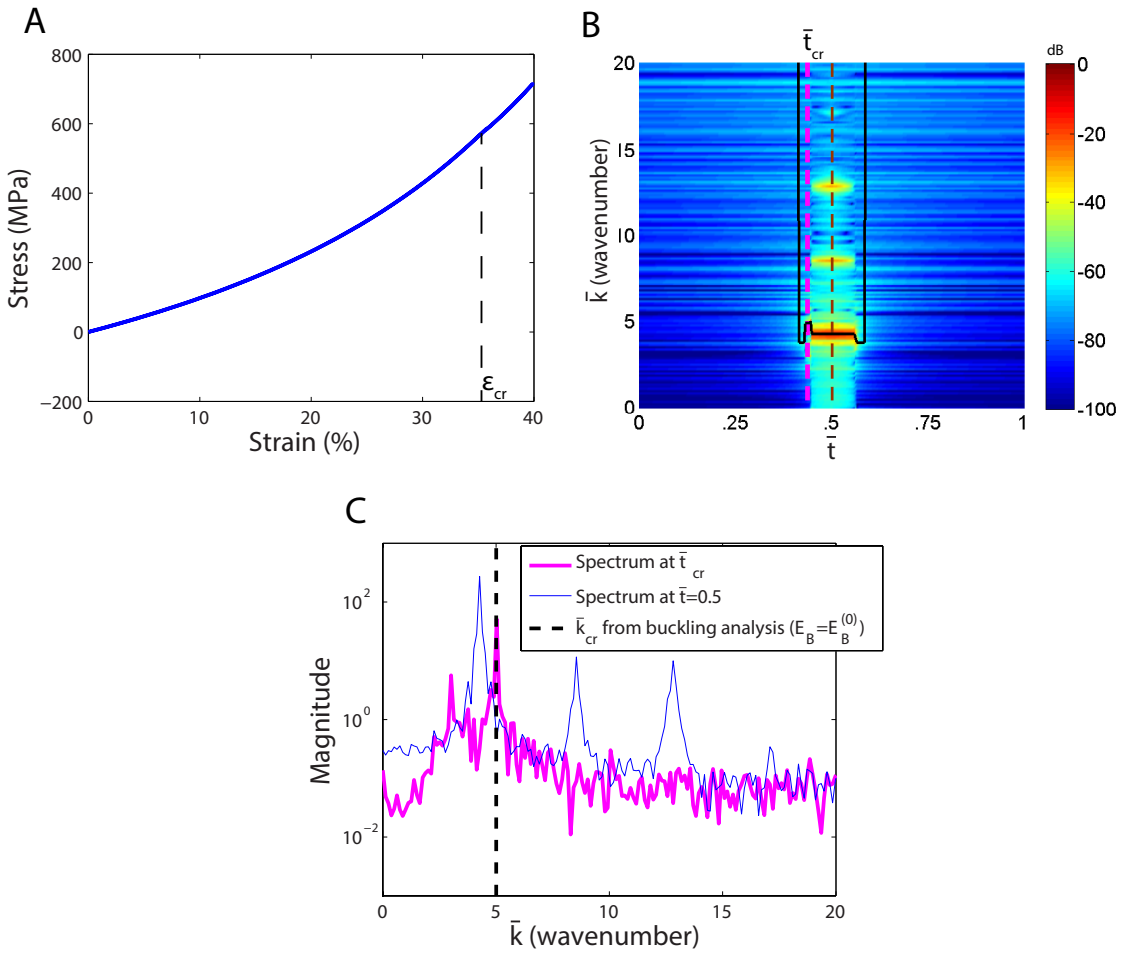

Figure 6.16: Modes and postbuckling for the transition volume fraction case for an elastic composite. A. Stress vs strain response. B. Nondimensional wavenumber spectrum vs normalized time. Dark black line refers to the maximum wavenumber at any given time. C. Nondimensional wavenumber spectrum at buckling and unloading. Dashed black lines refer to buckling wavenumber attained from linear buckling analysis.

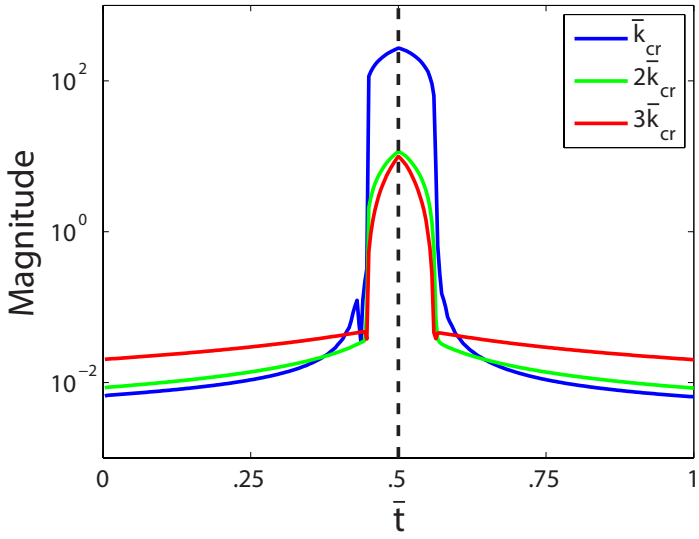

Figure 6.17: Magnitude of the wavenumbers that arise from harmonic distortion as a function of time for an elastic composite.

Chapter 7

Tunable Characteristics Under Periodic Loading

Using the theory from [1], the finite deformation response of non-dilute composites under periodic loading was studied. Because buckling has such a large effect on the stress vs strain response of viscoelastic layered composites, the effect of prestrain was also studied.

7.1 Effect on dynamic properties

Experimentally, dynamical mechanical analysis (DMA) is used to measure the mechanical properties that characterize the response of a material under periodic loading [20]. When loaded periodically with a prestrain, the strain is given by the following equation:

$$\begin{aligned} \varepsilon(t) &= \dot{\varepsilon}t \text{ if } 0 < t < t_r \\ &= \varepsilon_0 \text{ if } t_r < t < t_s \\ &= \varepsilon_0 + \Delta\epsilon \sin(2\pi f t) \text{ if } t > t_s \end{aligned} \tag{7.1}$$

where t_r is the rise time, t_s is the time of the start of the periodic loading, $\dot{\epsilon}$ is the strain rate ($\dot{\epsilon} = \epsilon_0/t_r$), ϵ_0 is the prestrain, f is the frequency of the cyclic loading and $\Delta\epsilon$ is the amplitude of the cyclic loading. $\epsilon(t)$ is represented graphically in Figs. 7.1A and 7.1B. In all the cases considered in this section, $\Delta\varepsilon$ is $1 \times 10^{-3}\%$, $f = 1$ Hz while ε_0 is varied. The numerical results at different frequencies would be qualitatively similar. The stress response for one particular case is shown in Figs. 7.1C and 7.1D. In this case, the nominal stress increases until the prestrain value is reached because the prestrain is below the critical strain. Then, as the strain is held constant, the stress gradually decreases and reaches a steady state value close to the initial value (due to viscoelastic stress relaxation). Periodic loading results in a hysteresis loop.

The dynamic Young's modulus, $|E^*|$, (which is a measure of stiffness under cyclic loading), and the loss factor, η (which is a measure of damping) were computed for the last cycle (Fig. 7.1D) of periodic loading using the equations given in Appendix B.

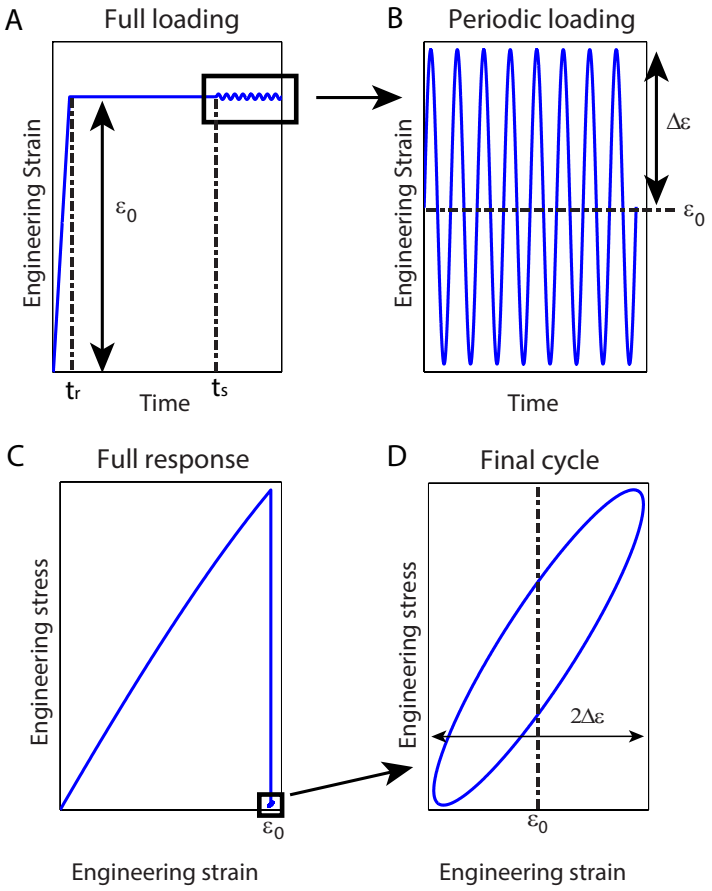

Figure 7.1: Engineering strain vs time for A. The entire loading cycle. B. The periodic loading. And the stress vs strain response for C. The entire loading cycle. D. The final cycle.

Since the buckling shape (Fig. 5.2A) of an initially vertical ($\theta_0 \approx 0$) and non-dilute composite is similar to the undeformed shape of a layered composite with $\theta_0 \neq 0$, the finite deformation simulation of cyclic loading with a prestrain for $\theta_0 \approx 0$ was compared to the linear viscoelastic theory (without prestrain) of composites with $\theta_0 \neq 0$. First, the value of the angle $\theta_s(\epsilon_0)$, that is reached after prestraining the initially vertical composite to a prestrain of value ϵ_0, was computed. This angle is

held constant until the stress relaxes to a constant value (see Fig. 7.2A). $|E^*|$ and η were computed using the linear viscoelastic theory for $\theta_0 = \theta_s(\epsilon_0)$ (Fig. 7.2B) by adapting the equations given in [27] to the plane strain case (see Appendix C).

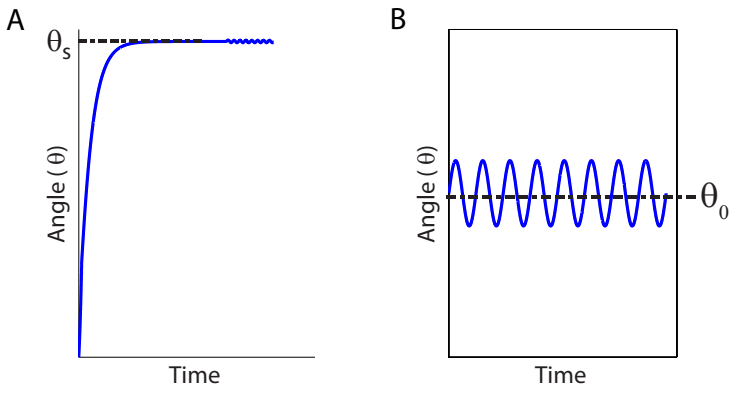

Figure 7.2: Angle, θ, vs time for A. Periodic loading after prestrain. After holding the strain at the prestrain value, θ converges to a constant value, θ_s. B. Periodic loading without prestrain with an initial angle, θ_0.

Figs. 7.3A and B show the stiffness and damping values as functions of prestrain, ϵ_0. As the prestrain is increased from 0 to 10%, the effective dynamic modulus decreases by two orders of magnitude and the damping increases by two orders of magnitude. These results are due to the rotation of the layers as the prestrain is increased. On the same graphs, the value obtained using the linear viscoelastic theory using an initial angle, $\theta_0 = \theta_s(\epsilon_0)$, are plotted as a function of ϵ_0. There is good agreement between the finite deformation theory and the linear viscoelastic theory with an initial angle.

The dynamic modulus is plotted as a function of the damping in the stiffness-loss map shown in Fig. 7.3C. Each point of each line corresponds to the values obtained for $|E^*|$ and η at a fixed prestrain value. As the prestrain is increased the points first move toward the right side of the figure (indicating a large increase in the damping and small reduction in the stiffness), before moving towards the bottom (indicating a large decrease in the stiffness and a small increase in the damping). The same effect is

obtained by simulating composites with increasing angle (in the small strain regime).

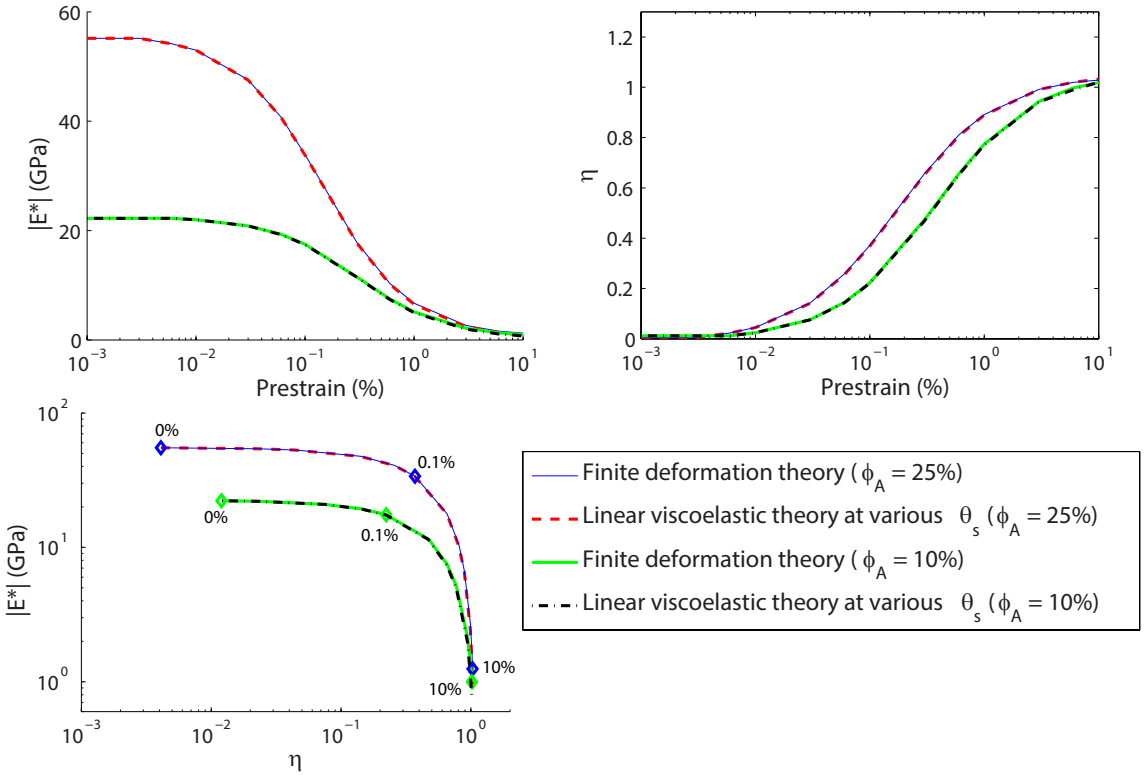

Figure 7.3: Comparison between the finite deformation theory and the linear viscoelastic theory for a composite with an initial angle $\theta_0 = \theta_s$. A. Dynamic modulus vs. prestrain. B. Damping vs. prestrain. C. Stiffness loss map for various volume fractions (points along each line are for varying ϵ_0). Values obtained for ϵ_0 =0, 0.1 and 10% are depicted by diamond symbols.

7.2 Conclusions

Meaud *et al.* [27] previously showed that simultaneous high stiffness and damping can be achieved in layered composites by choosing optimal values for the angle, θ, of the composite. These results show that similar properties can be achieved by the application of a prestrain. By applying a prestrain to the composite, the stiffness and damping can be tuned accordingly.

Chapter 8

Conclusions and Future Work

The main contribution of this work was to highlight the finite deformation response of parallel plane layered viscoelastic composites. Elastic buckling simulations guided the research to better understand the viscoelastic postbuckling response. Finite element analysis was used to validate theory that was discussed and derived in [1] and also to simulate the postbuckling response. Several conclusions were drawn in regards to the evolution of buckling:

1. The critical buckling strain, ϵ_{cr}, is dependent on the strain rate, $\dot{\epsilon}$: higher the $\dot{\epsilon}$, higher the ϵ_{cr}.

2. Viscoelastic composites can buckle with either a finite of an infinite wavelength. This is a function of the strain rate, the volume fraction, ϕ_A, of the stiff material and of the stiffness ratio between materials A and B.

3. Viscoelastic composites can be categorized into three different cases which were chosen to be called the non-dilute (infinite buckling wavelength), dilute (finite buckling wavelength) and transition (wavelength that can grow to an infinite length over time) cases. Classification is dependent on the stiffness and volume fraction of the stiff material.

Previous research showed that composites that had simultaneous high stiffness and damping were indeed possible by varying composite micro-structures. Using the validated theory from [1], this work showed that similar stiffness and damping characteristics of non-dilute viscoelastic composites are attainable by the application of a prestrain. This enables one to tune composites using the same composite microstructure.

All results presented in this thesis are based off theory and finite element simulations. Simulations with added imperfections were considered to provide a more realistic result. The effect of a finite height was considered in buckling simulations and for the non-dilute case, but not for the dilute case, which is a natural extension to this work. While developing theory and using simulations is helpful in any field of research and provides a solid foundation for the work, experimental results are invaluable. Using 3D printing, viscoelastic composites of a finite size can be printed and test experimentally to provide more insight into their finite deformation mechanics.

Appendix A

Abaqus material parameters

The variables displayed in Table 4.1 are those that are commonly used to describe materials. However, in ABAQUS, the values used to model the materials are different. These are displayed in Table A.1. The values in Table 4.1 can be transformed into what is needed in Table A.1 using equations A.1 and A.2.

Table A.1: Model parameters inputted in ABAQUS for material A and material B

Symbol	**Description**	**Value**
$C_{10}\|_A$	Related to shear modulus (compressible) Related to shear modulus (incompressible)	$38,461.54$ MPa $33,333.33$ MPa
$D_1\|_A$	Related to bulk modulus (compressible) Related to bulk modulus (incompressible)	1.2×10^{-5} 0
$C_{10}\|_B$	Related to long term shear modulus	0.5575 MPa
$D_1\|_B$	Related to long term bulk modulus	0
g_1	Related to viscoelastic branch shear modulus	0.992622 MPa
k_1	Related to viscoelastic branch bulk modulus	0
$\tau_B^{(\alpha)}$	Relaxation time constant	0.15 s

$$C_{10} = \frac{G}{2} \tag{A.1}$$

$$D_1 = \frac{2}{K} \tag{A.2}$$

Appendix B

Computation of stiffness and damping for the nonlinear case

When loaded periodically after application of a prestrain, the stress corresponding to the strain in Eq 7.1 can be written as:

$$\sigma(t) = \Delta\sigma \sin(\omega t + \delta) + \sigma_0 \tag{B.1}$$

where $\Delta\sigma$ is the amplitude of the stress curve while δ corresponds to the phase lag. σ_0 is the static stress value which occurs when the strain is equal to ε_0. Using the technique described below, determining the effective stiffness and damping when under this type of loading can be also be done for the case of a nonlinear response. The values obtained match the conventional definitions for linear viscoelastic materials at infinitesimal strains without prestrain.

B.1 Stiffness

In this research the effective stiffness of a layered viscoelastic composite is considered to be the absolute value of its dynamic modulus, $|E^*|$, which can be obtained graphically by analyzing the stress versus strain response of the composite. The overall effective stiffness is obtained by dividing the difference between the maximum and minimum values of the stress, $\sigma_{max} - \sigma_{min} = 2\Delta\sigma$, by the difference between the maximum and minimum value of the strain, $\epsilon_{max} - \epsilon_{min} = 2\Delta\epsilon$. $|E^*|$ corresponds to the slope of the line that connects the lower left corner to the upper right corner of the box as shown in Fig B.1A for a linear viscoelastic material. This graphical interpretation is extended to define the effective stiffness of a nonlinear viscoelastic material, as shown in B.1B [1].

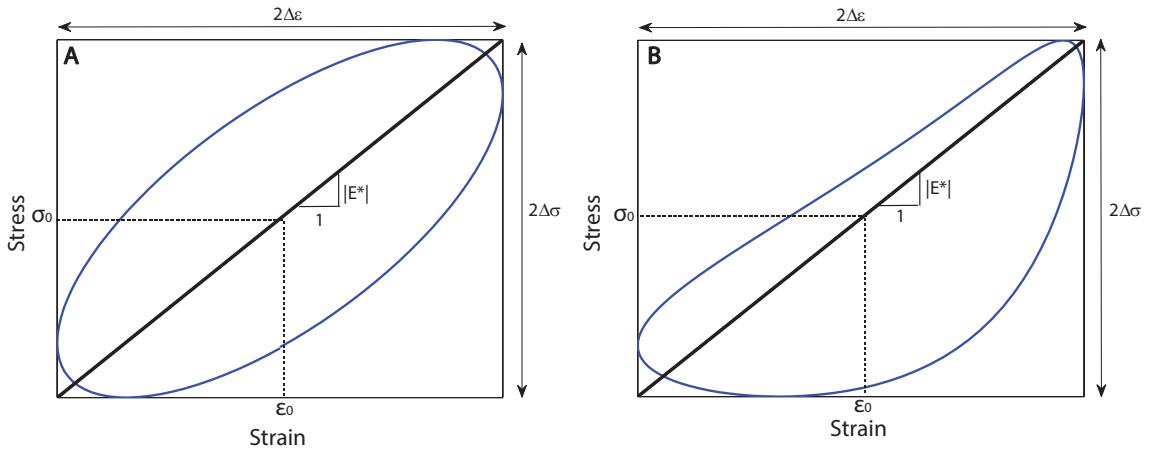

Figure B.1: Force displacement boundary along with line depicting the dynamic modulus, $|E^*|$. A. Shown for a linear viscoelastic material. B. Shown for a nonlinear viscoelastic material

B.2 Damping

In a nonlinear response, since the stress is no longer a periodic function of time, a general definition is needed. Damping is the energy that a material dissipates per cycle which can also be calculated using equation B.2.

$$W_d = \int_0^T \sigma(t) \frac{d\varepsilon}{dt}\, dt \tag{B.2}$$

Where $T = 2\pi/\omega$ is the period of the input. Computing the integral in Eq. B.2 gives:

$$W_d = \pi \Delta\varepsilon \Delta\sigma \sin(\delta) \tag{B.3}$$

Solving Eq. B.3 for $\tan(\delta)$ we get

$$\tan(\delta) = \tan\left[\sin^{-1}\left(\frac{W_d}{\pi \Delta\varepsilon \Delta\sigma}\right)\right] \tag{B.4}$$

Following the method described in Alur and Meaud [1], $\pi\Delta\varepsilon\Delta\sigma$ corresponds to the maximum energy per cycle that a linear viscoelastic material can dissipate for given

values of $\Delta\varepsilon$ and $\Delta\sigma$. This value is noted as $W_d^{max}(\Delta\varepsilon, \Delta\sigma)$. For a linear viscoelastic material $\tan(\delta)$ can also be written as:

$$\tan(\delta) = \tan\left[\sin^{-1}\left(\frac{W_d}{W_d^{max}(\Delta\varepsilon, \Delta\sigma)}\right)\right] \tag{B.5}$$

This is extended to define the effective loss factor for a nonlinear viscoelastic material, η, to be:

$$\eta = \tan\left[\sin^{-1}\left(\frac{W_d}{W_d^{max}(\Delta\varepsilon, \Delta\sigma)}\right)\right] \tag{B.6}$$

The energy dissipated, W_d, by a viscoelastic material can be obtained graphically by measuring the area within the stress-strain response, while $W_d^{max}(\Delta\varepsilon, \Delta\sigma)$ corresponds to the ellipse whose area is $\pi\Delta\epsilon\Delta\sigma$. This is graphically shown in Figs. B.2A and B.2B [1].

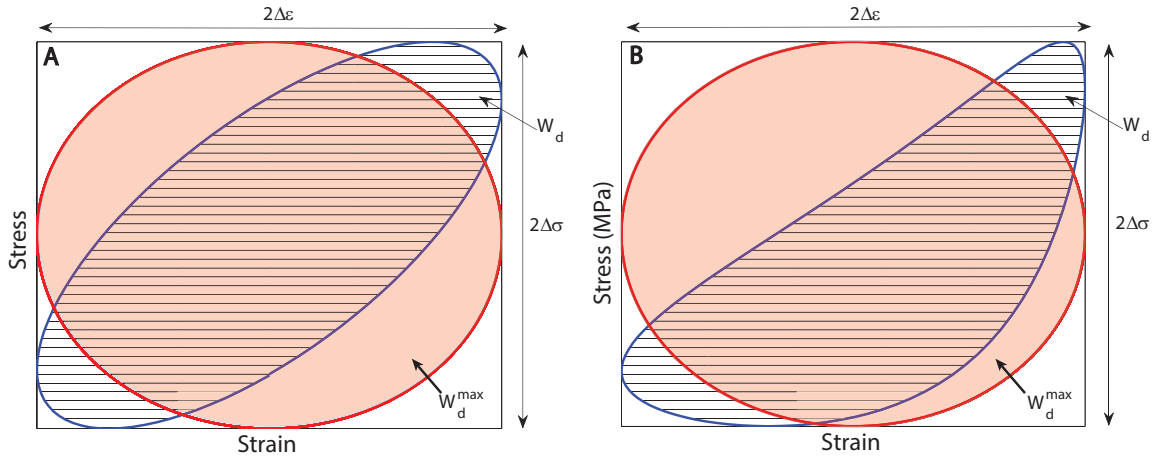

Figure B.2: Energy dissipated along with maximum energy dissipated within the same stress-strain boundary. A. Linear viscoelastic material. B. Nonlinear viscoelastic material.

Appendix C

Plane strain linear viscoelastic theory formulation

Meaud and Hulbert [26] derived the complex Young's moduli for Reuss composites (loading in the z direction, see Fig. 2.2) and Voigt composites (loading in the x direction) in response to dynamic loading. However, they did this for the generalized plane strain case (*i.e*, the out of plane dimension is assumed infinite such that the normal strains in the two phases are identical in the out of plane direction). In this research all simulations are in plane strain (*i.e*, the normal strains in the two phases are 0 in the out of plane direction). Applying the condition $\epsilon_y^A = \epsilon_y^B = 0$ to constitutive equations 10 and 13 from Liu *et al.* [24] in conjunction with equilibrium equations 15 through 17 and kinematic equations 18 through 20 the Young's modulus for the Reuss configuration, E_x^{eff}, was derived.

$$E_x^{eff} = \frac{E_A E_B}{\phi_A E_B + \phi_B\big(E_A(1-\nu_B^2) + E_B\nu_A(1+\nu_B)\big) + \frac{q_1\phi_B\nu_B\left(\nu_A E_B - E_A(1+\nu_B)\right)}{q_2}} \tag{C.1}$$

where q_1 and q_2 are:

$$q_1 = E_B\nu_A\phi_A(\nu_A+1) - E_A\nu_B\phi_A(\nu_B+1) \tag{C.2}$$

$$q_2 = E_B\phi_B(\nu_A^2-1) + E_A\phi_A(\nu_B^2-1) \tag{C.3}$$

To solve for E_y^{eff}, which corresponds to the Voigt configuration, the same constitutive equations were used but with equilibrium equations 23 through 25 and kinematic equations 26 through 28 from Liu *et al.* [24].

$$E_y^{eff} = \frac{\phi_A E_A}{1-\nu_A^2} + \frac{\phi_B E_B}{1-\nu_B^2} \tag{C.4}$$

The effective modulus in the Y direction is then computed using Eq. 15 given in [27].

Bibliography

[1] K. Alur and J. Meaud. Nonlinear mechanics of non-dilute viscoelastic layered composites. *International Journal of Solids and Structures*, Under review.

[2] M. Ashby. Overview no. 80: On the engineering properties of materials. *Acta Metallurgica*, 37(5):1273 – 1293, 1989.

[3] G. S. Bjorkman and J. M. Piotter. Finite element mesh considerations for reduced integration elements. *ASME 2008 Pressure Vessels and Piping Conference*, 2008.

[4] A. Browning, C. Ortiz, and M. C. Boyce. Mechanics of composite elasmoid fish scale assemblies and their bioinspired analogues. *Journal of the mechanical behavior of biomedical materials*, 19:75–86, 2013.

[5] C. P. Chen and R. S. Lakes. Analysis of high-loss viscoelastic composites. *Journal of Materials Science*, 28:4299–4304, 1993.

[6] Dassault Systmes. *ABAQUS User's Manual, Version 6.13*, abaqus 6.13 edition, April 2013.

[7] L. Dong and R. Lakes. Advanced damper with negative structural stiffness elements. *Smart Materials and Structures*, 2012.

[8] B. A. Fulcher, D. W. Shahan, M. Haberman, C. C. Seepersad, and P. WIlson. Analytical and experimental investigation of buckled beams as negative stiffness elements for passive vibration and shock isolation systems. *Journal of Vibration and Acoustics*, 2014.

[9] R. F. Gibson. A review of recent research on mechanics of multifunctional composite materials and structures. *Composite Structures*, 2010.

[10] Z. Hashin. Complex moduli of viscoelastic composites. fiber reincorced materials. *International Journal of Solids and Structures*, 1970.

[11] Z. Hashin. Complex moduli of viscoelastic composites. general theory and application to particulate composites. *International Journal of Solids and Structures*, 6(5):539–552, 1970.

[12] R. Huang. Kinetic wrinkling of an elastic film on a viscoelastic substrate. *Journal of the Mechanics and Physics of Solids*, 53(1):63–89, 2005.

[13] R. Huang and Z. Suo. Instability of a compressed elastic film on a viscous layer. *International Journal of Solids and Structures*, 39(7):1791–1802, 2002.

[14] R. Huang and Z. Suo. Wrinkling of a compressed elastic film on a viscous layer. *Journal of Applied Physics*, 91(3):1135–1142, 2002.

[15] S. Im and R. Huang. Evolution of wrinkles in elastic-viscoelastic bilayer thin films. *Journal of applied mechanics*, 72(6):955–961, 2005.

[16] T. Jaglinski, D. Kochmann, D. Stone, and R. Lakes. Composite materials with viscoelastic stiffness greater than diamond. *Science*, 2007.

[17] H. Kalathur and R. Lakes. Column ddamper with negative stiffness: high damping at small amplitude. *Smart Materials and Structures*, 2013.

[18] L. Kashdan, C. C. Seepersad, M. Haberman, and P. S. Wilson. Design, fabrications and evaluation of negative stiffness elements using sls. *Rapid Prototyping Journal,*, 18, 2012.

[19] D. Kochmann. Stable extreme damping in viscoelastic two-phase composites with non-positive-definite phases close to the loss of stability. *Mechanics Research Communications*, 2013.

[20] R. Lakes. *Viscoelastic materials*. Cambridge University Press, 2009.

[21] R. Lakes and W. Drugan. Dramatically stiffer elastic composite materials due to a negative stiffness phase? *Journal of Mechanics and Physics of Solids*, 2002.

[22] R. Lakes, T. Lee, A. Bersie, and Y. Wang. Extreme damping in composite materials with negative stiffness inclusions. *Nature*, 2001.

[23] Y. Li, N. Kaynia, S. Rudykh, and M. C. Boyce. Wrinkling of interfacial layers in stratified composites. *Advanced Engineering Materials*, 15(10):921–926, 2013.

[24] B. Liu, X. Feng, and S.-M. Zhang. The effective young's modulus of composites beyond the voigt estimation due to the poisson effect. *Composites Science and Technology*, 69(13):2198–2204, 2009.

[25] O. Lopez-Pamies and P. Ponte Castañeda. Microstructure evolution in hyperelastic laminates and implications for overall behavior and macroscopic stability. *Mechanics of Materials*, 41(4):364–374, 2009.

[26] J. Meaud and G. Hulbert. Dependence of the dynamic properties of voigt and reuss composites on the poisson's ratio and bulk loss factor of the constituent materials. *Journal of Composite Materials*, 47:3237–3247, 2013.

[27] J. Meaud, T. Sain, G. M. Hulbert, and A. M. Waas. Analysis and optimal design of layered composites with high stiffness and high damping. *International Journal of Solids and Structures*, 50(9):1342 – 1353, 2013.

[28] R. Parnes and A. Chiskis. Buckling of nano-fibre reinforced composites: a re-examination of elastic buckling. *Journal of the Mechanics and Physics of Solids*, 50(4):855–879, 2002.

[29] J. Reddy. *An Introduction To The Finite Element Method*. Tata McGraw-Hill, 2006.

[30] B. Rosen. Mechanics of composite strengthening. *Am. Soc. Metals Seminar, Fibre Composite Materials, Metals Park, Ohio*, pages 37–75, 1965.

[31] S. Rudykh and M. C. Boyce. Analysis of elasmoid fish imbricated layered scale-tissue systems and their bio-inspired analogues at finite strains and bending. *IMA Journal of Applied Mathematics*, doi: 10.1093/imamat/hxu005, 2014.

[32] S. Rudykh and M. C. Boyce. Transforming small localized loading into large rotational motion in soft anisotropically structured materials. *Advanced Engineering Materials*, 16(11):1311–1317, 2014.

[33] T. Sain, J. Meaud, B. Yeom, A. Waas, and E. Arruda. Rate dependent finite strain constitutive modeling of polyurethane and polymer-clay nano-composites. *International Journal of Solids and Structures*, 2015.

[34] Y. Wang and R. Lakes. Composites with inclusions of negative bulk modulus: extreme damping and negative poisson's ratio. *Journal of composite materials*, 2005.

[35] Y.-C. Wang and R. Lakes. Stable extremely-high-damping discrete viscoelastic systems due to negative stiffness elements. *Applied physics letters*, 84(22):4451–4453, May 2004.